Journal of Asian Earth Sciences 63 (2013) 112–129

Contents lists available at SciVerse ScienceDirect

Journal of Asian Earth Sciences

journal homepage: www.elsevier.com/locate/jseaes

Is the HP–UHP Hong'an–Dabie–Sulu orogen a piercing point for offset on the Tan–Lu fault?

Mary L. Leech [a,*], Laura E. Webb [b]

[a] Department of Geosciences, San Francisco State University, 1600 Holloway Avenue, San Francisco, CA 94132, United States
[b] Department of Geology, Delehanty Hall, University of Vermont, Trinity Campus, 180 Colchester Avenue, Burlington, VT 05405-1758, United States

ARTICLE INFO

Article history:
Available online 5 September 2012

Keywords:
Ultrahigh-pressure metamorphism
Hong'an–Dabie–Sulu
Tan–Lu fault
Eastern China
Collision model

ABSTRACT

The Tan–Lu fault is a major strike-slip fault in eastern China that appears to offset the high-grade rocks of the Hong'an–Dabie–Sulu orogen left-laterally ~540 km. We evaluate models for the collision between the South and North China blocks, published radiometric dates recording HP–UHP metamorphism and exhumation in the Hong'an–Dabie and Sulu terranes, and the timing of sinistral motion on the Tan–Lu fault to evaluate whether UHP rocks provide a piercing point for offset on the Tan–Lu fault. UHP metamorphism in Hong'an–Dabie was concurrent with Sulu based on U–Pb dating of coesite-bearing domains of zircon at 244 ± 5–226 ± 2 Ma for Hong'an–Dabie and 243 ± 4–225 ± 2 Ma for Sulu. Retrograde metamorphism began c. 220 Ma for both Hong'an–Dabie and Sulu, but retrograde zircon growth ended c. 214 Ma in Hong'an–Dabie and continued until c. 202 Ma in Sulu based on U–Pb dating of zircon domains external to coesite-bearing domains. Structures in Sulu are rotated 25° counter-clockwise from, but are broadly similar to, Hong'an–Dabie suggesting the two areas have a common Triassic orogenic history that pre-dates motion on the Tan–Lu fault, and that is consistent with paleomagnetic studies. We constructed a pre-Cretaceous restoration of the Hong'an–Dabie–Sulu belt that moves the Sulu terrane south, aligning the suture and the eclogite-facies isograd, and rotates Sulu c. 25° clockwise to re-align structures with Hong'an–Dabie. Our restoration is supported by published data and shows that the Hong'an–Dabie–Sulu orogen is a piercing point for post-collisional offset on the Tan–Lu fault and that these regions shared a common subduction–exhumation history. The Tan–Lu fault did not play a significant role in the Hong'an–Dabie–Sulu collision and likely developed later, in the Early Cretaceous.

1. Introduction

The Tan–Lu (or Tancheng–Lujiang) fault is a major structural feature in eastern China that appears to offset the high-grade rocks of the Hong'an–Dabie–Sulu orogen left-laterally some 550 km. The Tan–Lu fault may extend as much as 3600 km from south China (at the southern termination of the Dabie block) into the Bo Hai Sea across the Korean peninsula and northeast into the Sea of Okhotsk based on interpretation of satellite imagery (Okay and Sengor, 1992; Hsiao et al., 2004). Understanding the timing and magnitude of displacement on this fault has major implications for reconstructions of the Qinling–Dabie–Sulu orogen and thus our ability to understand the subduction–exhumation history of this archetypal ultrahigh-pressure (UHP) orogen.

A primary issue in evaluating the history of the Tan–Lu fault is whether or not the high-pressure (HP) and UHP rocks of the Dabie and Sulu terranes can be considered offset markers. The database of ages for HP–UHP rocks in the Sulu terrane has recently grown as a result of numerous publications since 2005 (e.g., Wallis et al., 2005; Yang et al., 2005; Hacker et al., 2006, 2009; Leech et al., 2006; Liu et al., 2006a,b,c, 2009a,b; Webb et al., 2006; Zhao et al., 2006a, 2007b; Gong et al., 2007; Cheng et al., 2008; Qiu et al., 2010; Liu and Liou, 2011; Schmidt et al., 2011); these data now make it possible to compare the timing of HP–UHP metamorphism and exhumation in the Sulu region to the ever-increasing database of ages for the Hong'an–Dabie area to the west (Fig. 1; e.g., Hacker and Wang, 1995; Hacker et al., 2000; Lin et al., 2005; Wan et al., 2005; Liu et al., 2006a,b; Ratschbacher et al., 2006). In this paper, we evaluate models for the collision between the South and North China Blocks (SCB and NCB), evaluate published radiometric dates recording suture zone HP–UHP metamorphism and exhumation of those rocks through the crust, and examine evidence for the age and extent of strike-slip motion on the Tan–Lu fault as it pertains to the Dabie–Sulu orogen. The goal is to develop a model for the collision of the SCB and NCB that integrates recent geo/thermochronology into with the existing body of paleomagnetic data constraining the collision, and that will allow us to determine whether the Tan–Lu fault formed during the collision and separated two related but independent Hong'an–Dabie and Sulu HP–UHP terranes,

* Corresponding author. Tel.: +1 415 338 1144; fax: +1 415 338 7705.
E-mail addresses: leech@sfsu.edu (M.L. Leech), lewebb@uvm.edu (L.E. Webb).

1367-9120/$ - see front matter © 2012 Elsevier Ltd. All rights reserved.
http://dx.doi.org/10.1016/j.jseaes.2012.08.005

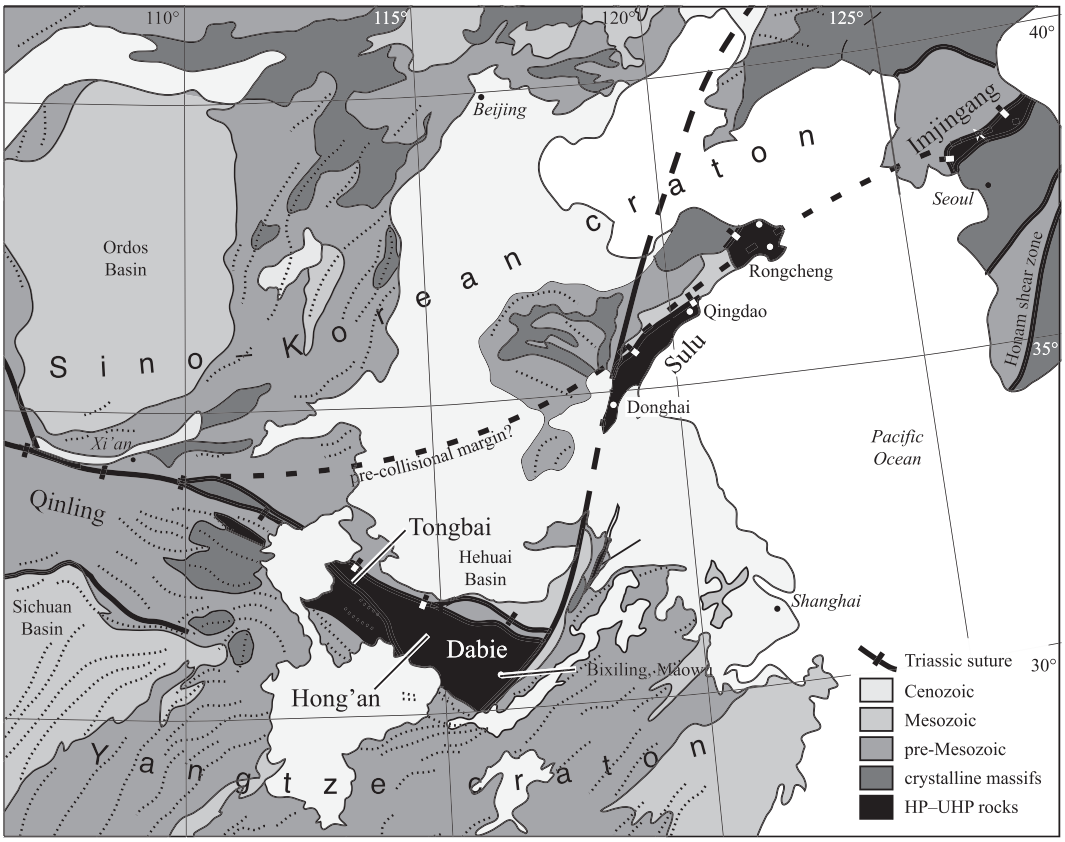

Fig. 1. Map of the Qinling–Tongbei-Hong'an-Dabie–Sulu–Imjingang orogen in eastern Asia showing the location of the Hong'an–Dabie areas, the Sulu area, and the Tan–Lu fault. Figure modified after Hacker et al., (2000, 2004). The South China Block comprises the Yangtze craton and the high-grade rocks of the Hong'an–Dabie and Sulu belts south of the Triassic suture; the North China Block refers to the region north of the suture.

or whether a continuous Hong'an–Dabie–Sulu HP–UHP belt is a piercing point for post-collisional offset on the Tan–Lu fault.

2. The Tan–Lu fault

The Tan–Lu fault was first recognized as an aeromagnetic anomaly in 1957 (Sun et al., 1993) and later correlation of high-grade rocks on both sides of the fault (the Dabie and Sulu regions) that truncate abruptly at the Tan–Lu fault identified it as a left-lateral strike-slip fault.

The Tan–Lu fault is a ~2 km-wide ductile shear zone best exposed east of the Dabie region and south of the Xiaotian–Mozitan fault (Fig. 1); this sinistral shear zone is comprised of multiple shear/mylonite zones that are from tens to hundreds of meters wide (Zhu et al., 2005). Normal faults related to development of the Qianshan basin truncate the eastern edge of the ductile shear zone (Zhu et al., 2005). Zhu et al. (2007) report phengite $^{40}Ar/^{39}Ar$ ages from mylonites in the southern Tan–Lu fault zone from 221–181 Ma interpreted to record cooling following syn-collisional shear in the Tan–Lu fault zone; these ages are significantly older than mica $^{40}Ar/^{39}Ar$ ages for mylonites of 150–102 Ma (Zhu et al., 2010), mica and hornblende $^{40}Ar/^{39}Ar$ ages for greenschist-facies mylonites in the southern part of the Tan–Lu fault zone between 143 and 125 Ma (Zhu et al., 2005), and $^{40}Ar/^{39}Ar$ whole-rock plateau ages of 132–120 Ma from a mylonite, ultramylonite, and phyllonite reported by Zhu et al. (2001, cit. in Zhu et al., 2005). Zhu et al. (2005) also report five $^{40}Ar/^{39}Ar$ biotite ages between about 120 and 110 Ma and one phengite age of 121 Ma that they interpret as cooling after slip. Other reported K–Ar ages of 110–90 Ma for fine-grained clays from fault gouge in the central part of the Tan–Lu fault and 103–95 Ma whole-rock ages from mylonites in the Zhangbaling area (Anhui region) may be cooling ages following earlier Mesozoic strike-slip motion, or may demonstrate that sinistral strike-slip motion continued through c. 100 Ma (Chen et al., 1989; Zhu et al., 2005). Two $^{40}Ar/^{39}Ar$ analyses of phengite from mylonites from the eastern margin of Dabie that yield ages of 239.8 ± 2.3 Ma and 240.8 ± 2.3 Ma are interpreted as a mixture of two generations of white mica and therefore geologically meaningless (Zhu et al., 2007). $^{40}Ar/^{39}Ar$ dating of white mica from Zhangbaling schist by Dunlap (2003) yielded plateau-like apparent age spectra interpreted based on X-ray diffraction and microstructural analyses to represent the timing of crystallization and cessation of greenschist-facies mylonitic deformation associated with transpression between 238.5 Ma and 235.4 Ma.

Apparent sinistral strike-slip faulting during the Mesozoic collision reversed slip sense sometime by the Late Cretaceous (Chen and Nabelek, 1987; Zhang et al., 2003); this change to dextral slip may be related to the oblique subduction of the Pacific plate after the SCB–NCB collision or escape tectonics related to the Himalayan orogeny (Gilder et al., 1999; Hsiao et al., 2004). The shift from sinistral transpression to dextral transtension may have occurred in the Early Cretaceous c. 145 Ma corresponding to the formation of rift basins along the Tan–Lu fault (see summaries in Ren et al., 2002; Zhu et al., 2010, and Zhang et al., 2003). $^{40}Ar/^{39}Ar$ ages for Tan–Lu mylonites older than ~145 Ma (see above) therefore likely record sinistral motion along the fault zone while younger ages record cooling associated with normal faulting. Cenozoic structures along the Tan–Lu fault zone vary along strike from high-angle normal, reverse, and thrust faults typical of strike-slip faults (Hsiao

et al., 2004; Lin et al., 2005). Frequent earthquakes and Quaternary deformation along the fault demonstrate the fault is still active (Hsiao et al., 2004).

Different authors have suggested varying amounts of offset on the Tan–Lu fault from ~150 km to a maximum of about 740 km (Sun et al., 1993) based on correlations of geologic units (high-grade rocks, volcaniclastic units, etc.) and/or the debated location of the suture between the SCB and NCB on either side of the fault zone. Gilder et al. (1999) states that uppermost Lower Cretaceous sediments along the Tan–Lu are not significantly offset and indicates the total sinistral offset was small and lasted ~18 Ma, likely ending at 99 ± 2 Ma based on a mean K–Ar date for mylonite in the Tan–Lu fault zone. Most of the sinistral displacement is likely concentrated between the Dabie block and the Shandong peninsula (see references in Sun et al., 1993, and Mercier et al., 2007) and therefore most estimates for maximum left-lateral slip are ~530 km based on the apparent offset of the high-grade rocks and the SCB–NCB suture. The suture is inferred to lie north of the Xiaotan-Mozitan fault on the northern margin of the Hong'an–Dabie block (Hacker et al., 2004) and to correspond to the Yantai–Qingdao–Wulian fault on the Shandong peninsula (e.g., Wang et al., 1989).

3. Review of paleomagnetic constraints on the SCB–NCB collision

Several papers discuss paleomagnetic data for eastern Asia in the latest Paleozoic and Mesozoic showing the relative positions of the NCB and SCB and degree of rotation of those blocks (e.g., Lin et al., 1985; Zhao and Coe, 1987, 1989; Lin and Fuller, 1990; Gilder et al., 1993, 1995, 1999; Gilder and Courtillot, 1997). These paleomagnetic models allow assessment of the timing of collision, the behavior of the NCB and SCB during exhumation of the high-grade rocks in the suture zone, and make predictions about the development of the Tan–Lu fault.

Lin et al. (1985) established that the SCB and NCB collided in the Triassic and were assembled as a single unit by the Middle Jurassic. Clockwise rotation of the SCB by ~50° about an Euler pole near the present-day north pole brings the path of the SCB and northern Eurasia into agreement. Lin and Fuller (1990) interpreted the Mesozoic SCB–NCB collision to have reactivated ancient faults in eastern China, converting some of them into strike-slip faults including the Tan–Lu fault. Paleomagnetic signatures suggest that the collision between the SCB and NCB started in the Early or Middle Triassic, and was complete in the Late Triassic–Early Jurassic. Further, they show collision started in the east and progressed west based on stratigraphic sequences in the Qinling fold belt, ages for HP metamorphic rocks, and dates for granite in the Qinling belt. The Zhao and Coe (1987) model also shows collision began in the east with closure progressing westward as the SCB rotates, but Permian paleomagnetic directions for the SCB and NCB are completely different prior to the Early Triassic with paleo-north showing that the SCB was rotated 60° clockwise with respect to the NCB.

The paleomagnetic data in Gilder et al. (1995) show Mesozoic poles for south China and south Korea coincide, implying that the SCB and Korea may have been part of the same continental landmass since the Triassic. The Triassic poles show a large amount of relative counterclockwise rotation required for the SCB before colliding with the NCB. Their collisional model relates the development of the Tan–Lu fault to the convergence and scissoring of the SCB (and Korea) with the NCB, and predicts that the motion along the Tan–Lu fault should terminate when the suturing was complete.

Data from Gilder and Courtillot (1997) require a scissor-like collision of the SCB and NCB that continued after the Early Jurassic and ended no later than the Late Jurassic based on the end of associated deformation at ~159 ± 9 Ma and when the poles of both plates are statistically identical. Rapid relative angular velocity (1°/Ma) between the SCB and NCB from 225 to 190 Ma coincides with post-UHP U–Pb and Ar/Ar dates from HP–UHP metamorphic rocks, implying syn-collisional rotational exhumation of high-grade rocks. Their data require that the SCB and NCB first collided near the eastern part of the suture in the Late Permian then progressively scissored together as the SCB rotated clockwise with respect to the NCB (similar to the Zhao and Coe, 1987, model); the progressive westward transition from marine to continental sedimentation along the suture supports this model as described in Yin and Nie (1993).

The model in Gilder et al. (1999) attributes counter-clockwise rotation of the NCB relative to the SCB during collision to left-lateral shear on the Tan–Lu fault, and Euler pole positions suggest at least 500 km of displacement on the Tan–Lu. In this model either UHPM occurred in situ in both the Dabie and Sulu areas and the Tan–Lu acted as a transform fault connecting two separate subduction zones, or UHPM rocks formed in the Dabie area were transported along the Tan–Lu after exhumation. This model suggests the Tan–Lu fault grew within the SCB as a corner on the NCB indented the SCB; folding in SCB cover rocks mark the paleo-NCB plate margin. One significant problem with the models shown in Gilder et al. (1999) is that the SCB does not collide with the NCB until the Late Triassic c. 10 Ma after UHPM took place in Dabie but could coincide with UHPM in Sulu (Leech et al., 2006); this could be resolved by extending the northern SCB continental margin which would allow an Early Triassic collision.

4. Models for SCB–NCB collision and the development of the Tan–Lu fault

Six end-member models have been proposed for the SCB–NCB collision, metamorphism and exhumation of HP–UHP rocks, and (perhaps most importantly here) the development of the Tan–Lu fault (Fig. 2; Okay and Sengor, 1992; Yin and Nie, 1993; Li, 1994; Xu and Zhu, 1994; Liou et al., 1996; Gilder et al., 1999). We review these end-member models including the predictions they make for exhumation of high-grade rocks and the timing of the formation of the Tan–Lu fault, then assess the models for agreement with radiometric age constraints and paleomagnetic data.

4.1. Continental transfer faults connecting two opposite-facing continental subduction zones (Fig. 2A)

Okay and Sengor (1992) proposed that the Tan–Lu fault is a post-collisional transfer fault connecting two continental subduction zones with opposite polarity (Fig. 2A). This model explains sinistral slip on the Tan–Lu fault with clockwise rotational motion of the SCB relative to the NCB with the fault playing a key role in exhuming UHP rocks. The Okay and Sengor (1992) model predicts that the two mountain belts should show opposite senses of coeval thrusting that produced post-collision exhumation of the UHP rocks and that Dabie and Sulu were each derived from the opposing crustal block, a potential modern analog in the Hindu Kush–Pamir (Chatelain et al., 1980; Roecker, 1982). However, seismic reflection imaging across the Dabie Shan and Xiaotian–Mozitan fault (interpreted as the suture zone between the SCB and NCB; Yuan et al., 2003) shows the SCB–NCB collision was a single, north-directed subduction zone, negating the Okay and Sengor (1992) collisional model.

4.2. Indenter models (Fig. 2B)

Several models for the SCB–NCB collision require a promontory on an irregularly-shaped SCB to explain the apparent northward

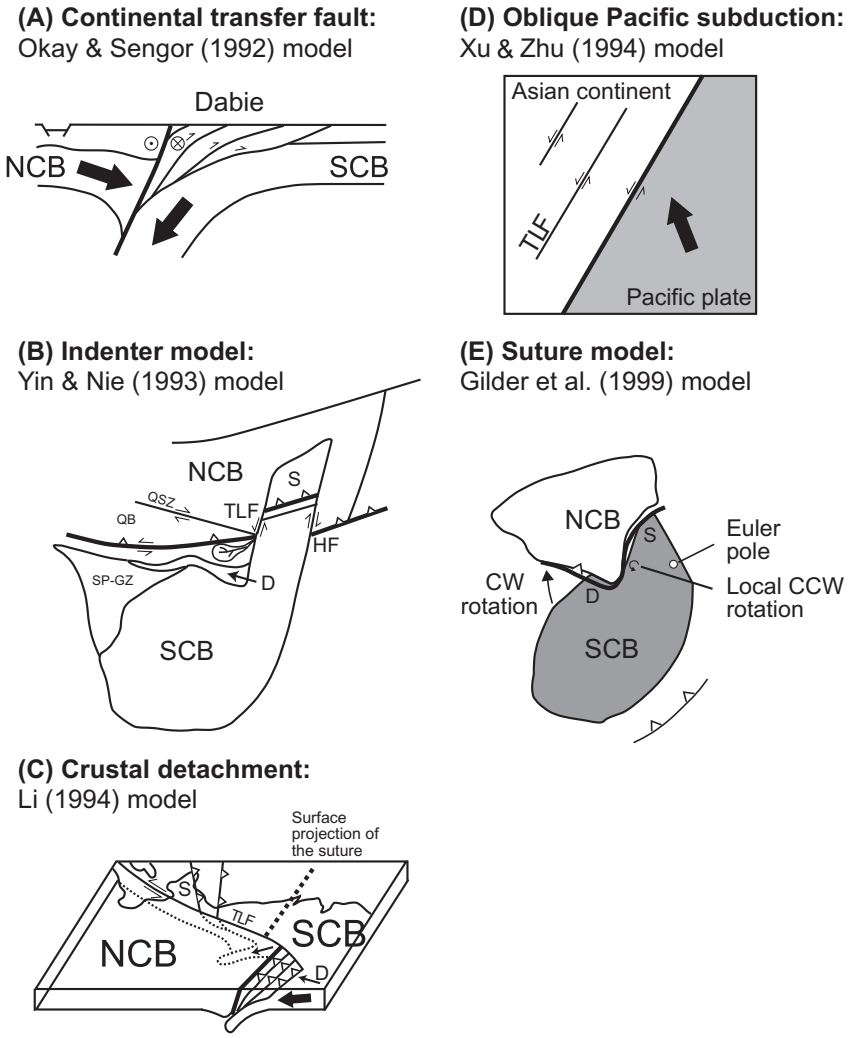

Fig. 2. Models for the SCB–NCB collision and development of the Tan–Lu fault. (A) Tan–Lu as a continental transfer fault between two opposite-facing subduction zones (Okay and Sengor, 1992); (B) SCB indenter model (Yin and Nie, 1993); (C) crustal detachment model (Li, 1994); (D) intracontinental transform fault from oblique Pacific subduction (Xu and Zhu, 1994); (E) clockwise rotation during collision/exhumation (Gilder et al., 1999). Cartoons are modified from original publications. D, Dabie; HF, Honam fault; QB, Qaidam basin; S, Sulu; SP-GZ, Songpan-Ganze; TLF, Tan–Lu fault.

offset of the high-grade rocks of the Sulu block (e.g., Yin and Nie, 1993). These promontories also appear prominently in models for paleomagnetic reconstructions of the collisional geometry and syn-collisional rotational exhumation of high-grade rocks (e.g., Gilder et al., 1999; Lin and Fuller, 1990).

Lin (1995) argues the collision of a promontory on the South China block is consistent with models showing collision first started in the east and that the lower crust of the South China block detached only east of the Tan–Lu fault, accounting for the abrupt termination of the Tan–Lu fault south of Dabie. Xu and Zhu (1994) show the northward projecting part of an irregular passive margin of the SCB extended some 500 km farther north than in the western part of the SCB before collision with the NCB; during collision the indenter was bound to the west by the Tan–Lu fault and to the east by the Honam shear zone similar to the model described by Yin and Nie (1993, 1996). A fundamental difference between these models and that of Okay and Sengor (1992) is that subduction was northward in both Dabie and Sulu and that collision began 10–20 Ma earlier in Sulu. Currently, little structural or geochronological data support Triassic motion along the Tan–Lu fault, and Gilder et al. (1999) criticized this idea because significant folding of Phanerozoic rocks is absent on the Shandong peninsula in the northern part of the Sulu belt. Instead, Gilder et al. (1999) proposed that the NCB indented the SCB in the Early to Middle Jurassic after exhumation of the UHP rocks, leading to bending of the SCB fold belt, formation of the Tan–Lu fault, and 70° of relative rotation between the NCB and SCB (Zhao and Coe, 1987). Later, Maruyama et al. (1997) stated that no sinistral offset is implied by an indenter model.

Yin and Nie (1993) proposed the NCB continental margin was arcuate like many active margins, and that the SCB had an irregular shape like other passive margins. Their model shows the eastern part of the SCB extended ~500 km further north than the west. As a result, the SCB–NCB collision began in the east at the Shandong peninsula (which later became the Sulu area) and progressed westward to Dabie and Qinling, implying that HP–UHP rocks in Sulu are older and those in Dabie–Qinling are younger. The indentation of the NE part of the SCB created the sinistral Tan–Lu and dextral Honam faults now bounding the Sulu terrane. Yin and Nie (1993) also point to evidence from the sedimentary record showing diachroneity in the collision, looking at the change from marine carbonate to clastic sedimentation: 258–248 Ma syn-collisional sediments are deposited on the SCB whereas clastic sediments are not deposited on the NCB until the Late Triassic (231–213 Ma). This diachroneity supports the model of Mattauer et al. (1991) that also shows collision progressing from east to

west. One problem with the Yin and Nie (1993) model is that paleomagnetic data show that with the required rotation, an SCB indenter poses an impossible space problem (Fig. 2E; Gilder et al., 1999).

4.3. Crustal detachment model (Fig. 2C)

Li (1994) proposed a crustal detachment model for the collision between the SCB and NCB east of the Tan–Lu fault based on linear aeromagnetic anomalies, field geology, and seismic profiling. Later adopted by Lin (1995) and Chung (1999), this model shows the upper crust of the SCB in the Subei-Yellow Sea region detached from the lower crust and was thrust >400 km over the NCB while the lower part of the lithosphere was subducted under the NCB along a subsurface suture (Fig. 2C) where the sinistral offset of the SCB–NCB suture is only 110–120 km in the deep crust. This model also shows collision beginning in the east. The interpretation that the aeromagnetic signature of the SCB–NCB suture extends with minor offset across the Tan–Lu fault suggests that the mantle suture is not offset by the Tan–Lu fault and that the Sulu orogen is the northern edge of a "crustal flake" of the SCB that was thrust some 400 km north over the NCB. This model implies that the UHP rocks of the Sulu region were initially part of the SCB and were subducted and exhumed prior to becoming part of the sheet thrust northward over the NCB.

4.4. Oblique Pacific plate subduction (Fig. 2D)

Xu and Zhu (1994) proposed a model in which the Tan–Lu fault is a major sinistral strike-slip fault that developed on the inner, continental side of a Eurasian-Pacific plate collision post-dating the SCB–NCB collision. In this model, the development of the Tan–Lu fault is attributed to oblique motion of the Pacific plate in the Late Jurassic to Early Cretaceous, or that the Pacific margin during that time was a transform fault (Xu, 1993; Xu and Zhu, 1994) similar to the San Andreas fault.

A related model proposed by Mercier et al. (2007) shows a NNE-oriented Tan–Lu margin connected two collisional margins located north of the Dabie and Sulu belts. In the Middle–Late Triassic, the SCB was obliquely subducted beneath the NCB along the Tan–Lu margin that acted as a compressional transfer zone between Dabie and Sulu. This model shows the southern Tan–Lu fault initiated in the Early Jurassic and acted as a sinistral transform fault during the Jurassic, until the SCB–NCB collision ended.

4.5. Suture model (Fig. 2E)

Xu and Zhu (1994) interpret the Tan–Lu fault either as a suture zone between the SCB and the NCB, a suture between the NCB and other terranes, or as a transform plate boundary. Zhang (1997) agrees that the Tan–Lu fault was part of an initial suture zone between the SCB and NCB explaining its abrupt termination at both the northern and southern ends of the fault, and contractional deformation within the fault zone and on both sides of the fault. This model (Fig. 2E) shows a rotational collision first in the east with clockwise rotation and final collision in the west like the models of Lin and Fuller (1990) and Gilder et al. (1999).

Ratschbacher et al. (2003) and Hacker et al. (2004) show that offset between Dabie and Sulu results from motion on the Tan–Lu from the Cretaceous to Cenozoic combined with post-collisional extension north of Dabie. They show 60° of relative rotation between the SCB and NCB in the Middle Triassic to Middle Jurassic with collision ending by the Late Jurassic using data from Zhao and Coe (1987) and Gilder and Courtillot (1997). The Hacker et al. (2004) model shows transpression during clockwise syn-collisional rotation of the SCB and exhumation of HP–UHP rocks resulting from a retreating plate boundary and syn-rotational extension. In the Hacker et al. (2004) model, a triangular-shaped plate margin on the SCB (similar to the eastern SCB in Fig. 2E) results in the eastern part of the Qinling–Dabie block subducted earliest and to greater depths than the Qinling area; stretching lineations in the Hong'an–Dabie area show clockwise rotation interpreted as rotation during exhumation by pivoting at a shallow point to the west for the portion of the orogen west of the Tan–Lu fault.

4.6. Post-collisional model for the development of the Tan–Lu fault

The structures and ages for HP–UHP rocks in Sulu are broadly similar to those found in the Hong'an and Dabie blocks ~550 km to the south suggesting the two areas have a common subduction/exhumation history that pre-dates motion on the Tan–Lu fault; the Tan–Lu fault may have behaved as a sinistral transfer fault between the Sulu and the Qingling-Hong'an–Dabie belts following Triassic collision of the SCB–NCB (Liou et al., 1996).

Previously published models explaining the offset between Dabie and Sulu as the result of post-collisional offset on the Tan–Lu fault (e.g., Kimura et al., 1990) make no predictions regarding the timing of exhumation of UHP rocks, and have been criticized on stratigraphic grounds (Yin and Nie, 1993). More recent additions to the database of radiometric ages for HP–UHP rocks in the Sulu block now allow better evaluation of the various model for the SCB–NCB collision. We discuss post-collisional models further following the review of published radiometric data.

5. Timing of HP–UHP metamorphism and exhumation in the Dabie–Sulu orogen

Numerous previous studies address the timing of prograde, UHP, and retrograde metamorphism in both the Dabie and Sulu regions. We summarize those results here, and focus on those dating results that most accurately record those stages in the subduction–exhumation evolution of the orogen.

5.1. Hong'an–Dabie

5.1.1. Prograde metamorphism (257–242 Ma)

Best estimates for prograde eclogite-facies metamorphism are based on U–Pb SHRIMP dating of quartz-bearing zircon domains contained within coesite-bearing domains that grew during UHP metamorphism yielding ages of 244 ± 4 Ma (10 spots, MSWD = 0.6; Liu et al., 2006b), 245 ± 4 Ma (13 spots, MSWD = 1.4; Liu et al., 2007), and 248 ± 11 Ma and 242 ± 5 Ma (Liu and Liou, 2011). The timing of prograde metamorphism is further constrained by Lu–Hf dating of garnet (257.4 ± 1.4 Ma) and Sm–Nd garnet-whole rock ages (252.5 ± 2.7 Ma) for oceanic eclogites from a mélange north of the western part of the Dabie (Cheng et al., 2010), as well as U–Pb dating of titanite interpreted as prograde (244 ± 3 Ma; Wawrzenitz et al., 2006).

5.1.2. UHP Metamorphism (244–226 Ma)

UHP metamorphism took place between 244 ± 5 and 226 ± 2 Ma based on U–Pb dating of coesite-bearing domains in zircon: 235 ± 7–233 ± 9 Ma from three different samples (Liu and Liou, 2011) and 235 ± 3 Ma (15 spots, MSWD = 1.2; Liu et al., 2007) for eclogites; 243 ± 1 Ma and 228 ± 2 Ma for jadeite quartzites (Liu and Jian, 2004); 244 ± 5 Ma and 226 ± 2 Ma for granitic gneisses (Wan et al., 2005); and 232 ± 4 Ma for dolomitic marble (Liu et al., 2006b). The timing of eclogite-facies metamorphism (not necessarily UHP eclogite-facies) has been estimated from garnet-only Sm–Nd data for 6 eclogites and one garnet peridotite that form an isochron at 225 ± 7 Ma (Chavagnac and Jahn, 1996); this is

the same age within error as an 8-point Sm–Nd isochron from Cheng et al. (2008) that gives an age of 217.6 ± 6.1 Ma for whole rock, garnet, kyanite, and omphacite fractions.

5.1.3. The end of UHP metamorphism and retrograde metamorphism associated with exhumation (220–214 Ma)

Zircon domains external to a coesite-bearing domain give ages of 220 ± 2 Ma, 217 ± 6 Ma, and 215 ± 6 Ma (10 spots, MSWD = 2.9) for eclogite (Liu et al., 2007, 2011; Liu and Liou, 2011), and 214 ± 5 Ma for marble (Liu et al., 2006b). Similar ages are reported for amphibolite-facies zircon rims dated at 220–214 Ma (Maruyama et al., 1998, cit. in Hacker et al., 2006).

UHP metamorphism must have been complete when granitic magmatism began: Most granitoids are Late Jurassic to Early Cretaceous (e.g., Ma et al., 1998; Zhao et al., 2004; Xu et al., 2007) except for one Late Triassic $^{40}Ar/^{39}Ar$ date for hornblende of 227.3 ± 7.6 Ma from a quartz monzonite in eastern Dabie near the Tan–Lu fault (Ma et al., 1998). $^{40}Ar/^{39}Ar$ thermochronologic and structural studies indicate that cooling below ~300 °C following exhumation and retrograde metamorphism at amphibolite-facies conditions was achieved by the Early Jurassic and that the bulk of the exhumation was associated with normal-sense top-to-the-north shear (e.g., Webb et al., 1999; Hacker et al., 2000).

5.2. Sulu

5.2.1. Prograde metamorphism (247–244 Ma)

U–Pb SHRIMP ages of 247 ± 4 Ma (9 spots; Liu et al., 2006b) and 244 ± 4 Ma (16 spots, MSWD = 0.8; Liu et al., 2007) were reported for zircon in quartz-bearing domains internal to coesite-bearing domains. These are the only Triassic ages reported for such low-pressure domains in zircon that contain coesite.

5.2.2. UHP Metamorphism (243–225 Ma)

The timing of UHP metamorphism in Sulu is based on dating of zircon domains with eclogite-facies and UHP inclusions that give ages that span a range from 243 ± 4 to 225 ± 2 Ma: Dated zircon domains containing coesite yield ages of 233 ± 4 Ma (12 spots, MSWD = 2.4; Liu et al., 2007) and 235 ± 9 Ma (2 spots, MSWD = 0.01; Liu and Xu, 2004) for eclogite; 233 ± 3 Ma for dolomitic marble (Liu et al., 2006b); 228 ± 5 Ma and 232 ± 4 Ma for para/orthogneiss (Liu et al., 2004a); 227 ± 9 Ma (Liu et al., 2005), 233 ± 5 Ma (6 spots from two samples, MSWD = 0.1; Liu and Xu, 2004), ages ranging from 235 ± 5 Ma to 225 ± 7 Ma (Liu and Liou, 2011), and 227 ± 2 (Liu et al., 2004b) for gneisses and a quartzite; and 231 ± 3 Ma and 233 ± 3 Ma for amphibolites (mean ages for zircons ranging from 243 ± 4 Ma to 225 ± 4 Ma; Liu et al., 2008). Garnet- and omphacite-bearing zircon domains from eclogites give ages of 243 ± 1 Ma and 227 ± 1 (Liu et al., 2006a) and 225 ± 2 (Zhao et al., 2007b), constraining eclogite-facies metamorphism but not necessarily UHP metamorphism. Other U–Pb zircon ages in the same range are from eclogites, peridotites, and a dunite (Yang et al., 2003; Liu et al., 2006a; Zhao et al., 2006a), and two gneisses (Tang et al., 2008).

Four Sm–Nd ages corresponding to the UHP event come from eclogites in areas where coesite has been identified: 221 ± 6 Ma from Li et al. (1993; 2-point isochron for Grt-Omp); 228 ± 6 from Li et al. (1994; 3-point isochron for Grt-Ph-WR); 221 ± 7 Ma from Schmidt et al. (2008; 3-point isochron for Grt-Cpx-WR); and 226 ± 4 Ma from Li et al. (1994; 4-point isochron for Grt-Omp-Ph-WR). These correspond well with eight Lu–Hf Grt-Cpx ages for eclogites of 222.7 ± 1.6–215.9 ± 1.3 Ma from Schmidt et al. (2008, 2011). These Sm–Nd and Lu–Hf ages for eclogites span a range from 221 ± 7 Ma to 228 ± 6 Ma, overlapping somewhat with ages for coesite-bearing zircon domains.

5.2.3. The end of UHP metamorphism and retrograde metamorphism associated with exhumation (219–202 Ma)

Zircon domains with low-pressure inclusions including quartz external to coesite-bearing zircon domains have been dated at 213 ± 6 Ma (Liu et al., 2006b), 208 ± 4 and 213 ± 5 (Liu et al., 2004a), 209 ± 3 Ma (Liu et al., 2004b), 213 ± 5 Ma (3 spots for two samples, MSWD = 0.3; Liu and Xu, 2004), 214 ± 5 Ma (8 spots, MSWD = 0.8; Liu et al., 2007), and ages ranging from 215 ± 5 to 202 ± 4 Ma for six different samples are interpreted as marking an amphibolite-facies retrogression. Liu et al. (2008) dated small, retrograde zircons coexisting with coesite-bearing zircon at 215 ± 3 Ma and 214 ± 4 Ma (mean ages for dates ranging from 219 ± 4 Ma to 205 ± 3 Ma).

Hacker et al. (2009) use the timing of oldest granitic plutons and dikes in northern Sulu to mark the definitive end of UHPM, with ages constrained by U–Pb zircon ages with errors <2 Ma: four ages from 226.2 ± 1.7 to 220.0 ± 1.8 Ma for granitic plutons (Chen et al., 2003; Wallis et al., 2005); 206.7 ± 1.9 (Wallis et al., 2005); and 205 ± 5 Ma from a dike (Chen et al., 2003). $^{40}Ar/^{39}Ar$ ages from a pyroxene syenite include a hornblende age of 214.6 ± 0.6 Ma and a K-feldspar age of 214.4 ± 0.3 Ma from the same pluton (Yang et al., 2005). Combined $^{40}Ar/^{39}Ar$ thermochronologic and structural studies indicate that cooling below 300 °C following exhumation and retrograde metamorphism at amphibolite-facies conditions in the Sulu region was achieved by the end of the Late Triassic and associated with normal-sense top-to-the-NW shear (e.g., Faure et al., 2003; Webb et al., 2006).

6. Comparing Dabie and Sulu dating

The compilation of geo/thermochronology data shows similarities in the timing of UHP metamorphism and possible differences in the timing of cooling and tectonic exhumation via normal-sense shearing of HP–UHP rocks in Sulu and Hong'an–Dabie regions (Fig. 3, Tables A1 and A2; see also Leech et al., 2006; Webb et al., 2006).

Fig. 3A shows probability density curves for published U–Pb, Lu–Hf, Sm–Nd, Rb–Sr, and $^{40}Ar/^{39}Ar$ ages in the Sulu areas (for ages used and references, see Table A1), and Fig. 3B shows the corresponding data for Hong'an–Dabie (Table A2). While there is considerable overlap for all radiometric data, there is generally greater spread in the ages obtained for the Hong'an–Dabie region. Well-constrained dating of amphibolite-facies retrograde metamorphism indicates the timing of cooling/exhumation ($^{40}Ar/^{39}Ar$ dating) may have began earlier in the Hong'an–Dabie area compared to Sulu. The data generally suggest that peak metamorphism began for both Hong'an–Dabie and Sulu by c. 244–243 Ma with exhumation of UHP rocks underway or ongoing by ~220 Ma. Exhumation may have been slower for Sulu, lasting until c. 202 Ma, whereas Hong'an–Dabie may have passed through the mid-crust by c. 214 Ma based on retrograde zircon growth.

Fig. 4 compares P–t and T–t paths for Dabie and Sulu: Dabie experienced cooling during decompression from UHP conditions to the middle crust while Sulu underwent isothermal decompression during exhumation from upper mantle depths to the lower crust (also supported by the numerical modeling of Li and Gerya, 2009) followed by a period of cooling during decompression to the mid-crust. The T–t path that Sulu followed implies rapid early exhumation along the subduction channel to mid-crustal depths followed by slower exhumation with concomitant cooling to the upper crust, similar to the Dabie area.

Cretaceous $^{40}Ar/^{39}Ar$ ages feature prominently in the Dabie data and are less significant in Sulu; this likely demonstrates the greater abundance of granitoid intrusions in the Dabie-Hong'an area and

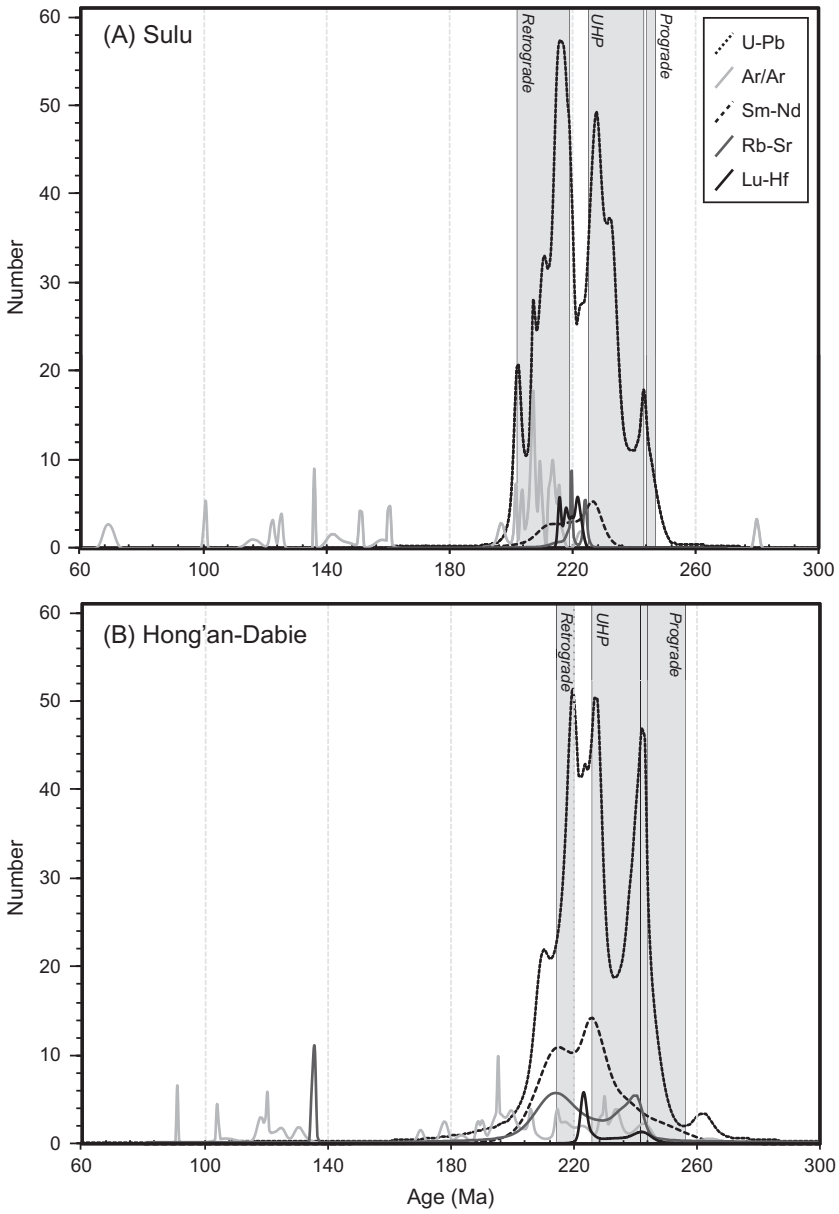

Fig. 3. Probability density curves for published U–Pb, Lu–Hf, Sm–Nd, Rb–Sr, and $^{40}Ar/^{39}Ar$ data for the UHP units of the Hong'an–Dabie and Sulu areas. (A) Ages for Sulu area. (B) Ages for Hong'an–Dabie area. References are listed in Tables A1 and A2. Curves for Rb–Sr and Lu–Hf are shown at 2× vertical scale for clarity.

greater exhumation associated with Early Cretaceous extension (e.g., Hacker et al., 1995).

7. Structure of the Dabie–Sulu orogen

The regional structure of the Sulu terrane is strikingly similar to that of Hong'an and Dabie Shan: The high-grade rocks of the Sulu terrane are characterized by a generally SE-dipping foliation, SE-plunging stretching lineations, and top-to-the-NW shear sense (Wallis et al., 1999; Faure et al., 2003; Webb et al., 2006; Xu et al., 2006). Deformation was accompanied principally by recrystallization under amphibolite-facies conditions. Structural variability within the UHP unit includes: (1) top-to-the-S sense of shear and S plunging stretching lineations in L–S tectonites in southern Sulu; and (2) both top-to-the-NW and top-to-the-W sense of shear and E- to SE-plunging stretching lineations in central Sulu. Top-to-the-SE shear sense was recognized in the high-pressure unit by Faure et al. (2003) and Xu et al. (2006) and was proposed to represent rare vestiges of deformation during subduction.

The orogen-scale structure of Hong'an–Dabie is an antiform: both the Hong'an–Dabie and Sulu areas display SE- to SW-dipping foliation, SE-plunging lineation, and top-to-the-NW shear sense (Hacker et al., 2000; Webb et al., 2001; Faure et al., 2003). Northern Hong'an differs where the south-oriented structures roll over into N- to NW-dipping foliations, N- to NW-plunging lineations, and N- to NW-directed sense-of-shear. Hong'an preserves the NW-trending km-scale synformal–antiformal structure of the metamorphic rocks unlike Dabie where there was extensive Cretaceous magmatism and extension along the north-dipping Xiaotian–Mozitan fault (Hacker et al., 2000; Ratschbacher et al., 2000; Webb et al., 2001).

Seismic reflection profiling across both Sulu and Dabie shows the antiformal structure of the UHP rocks extends to a depth of 20–30 km (Yuan et al., 2003; Xu et al., 2009). The reflection geometry in both areas shows a crustal-scale dome sits above

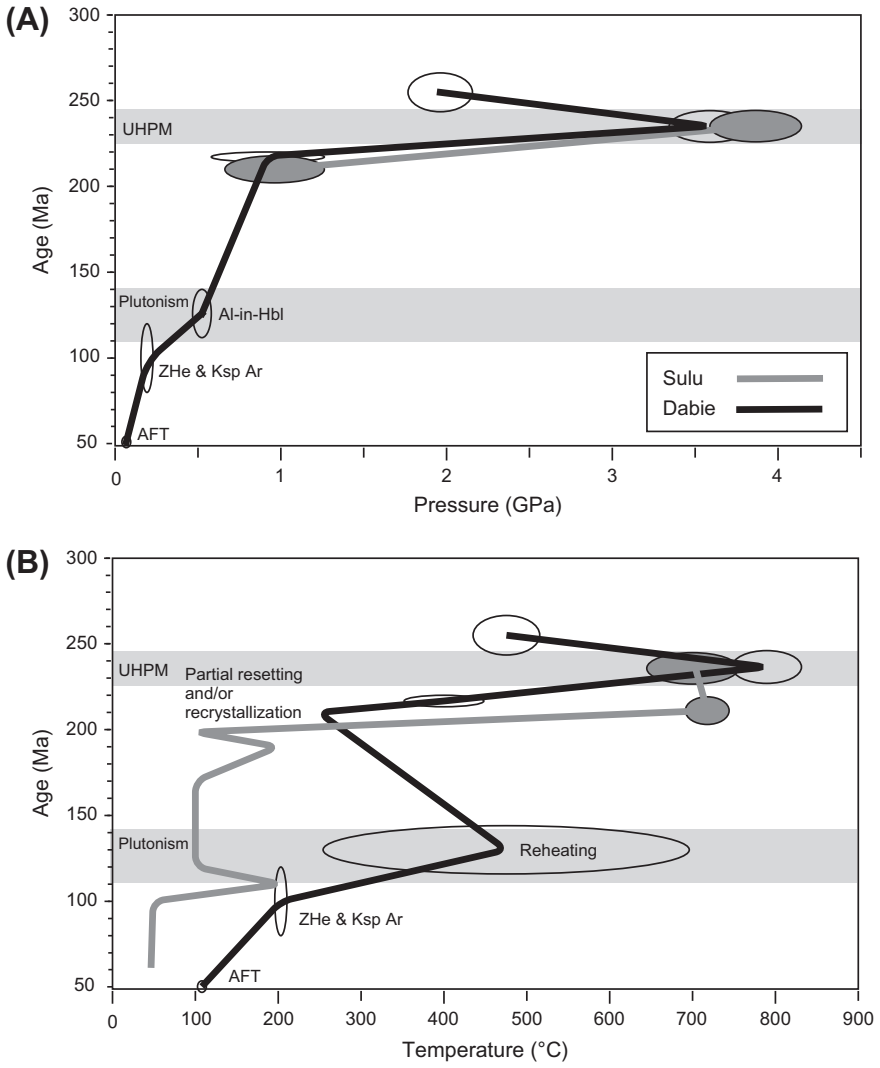

Fig. 4. Age–pressure and age–temperature plots for Hong'an-Dabie and Sulu subduction–exhumation histories. Both Hong'an-Dabie and Sulu areas followed near-identical pressure histories (A) but quite different cooling paths (B). Sulu shows near-isothermal decompression through from UHP conditions to mid-crustal levels (800–700 °C) while Hong'an-Dabie displays greater cooling during decompression. Prograde, UHP, and amphibolite-facies metamorphic conditions for the Hong'an-Dabie and Sulu terranes are based on those recalculated by Hacker et al. (2006) using net-transfer equilibria for original published data (see references in Hacker et al., 2006); the cooling path for Sulu is based on multi-domain diffusion modeling of K-feldspar (Webb et al., 2006) and modeling of apatite fission-track data from Liu et al. (2009c) for the lowest temperature segments. Reheating temperatures and pressures estimated from Al-in-hornblende barometry for Cretaceous plutonism from Ratschbacher et al. (2000). U–Th/He dating of zircon, $^{40}Ar/^{39}Ar$ dating of K-feldspar, and apatite fission-track ages are from Reiners et al. (2003). Ages for prograde, UHP, and amphibolite-facies retrograde metamorphism are based on U–Pb ages of coesite-bearing domains in zircon and domains internal and external to the coesite-bearing domains as discussed in this paper.

a sub-horizonal Moho, preserving a collisional structure that has been modified by syn- and post-orogenic processes (Yuan et al., 2003; Xu et al., 2009). Based on the seismic profiling, Yuan et al. (2003) suggests that UHP rocks returned to the surface by ductile flow of middle and lower crust laterally from the margins of the orogen, and by brittle upper crustal faults that extend into the ductile middle crust similar to metamorphic core complexes.

8. Discussion

Can the UHP rocks of the Hong'an–Dabie–Sulu belt be used as a piercing point for offset on the Tan–Lu fault? Or do the data demand that the Hong'an–Dabie and Sulu regions were separated by a syn-collisional Tan–Lu fault and underwent independent subduction–exhumation histories? Any model put forth to answer this question must honor well-established constraints regarding the Triassic SCB–NCB collision and the subsequent exhumation of the UHP units:

The proposed younging and westward migration shown in several models for the SCB–NCB collision (e.g., Zhao and Coe, 1987; Yin and Nie, 1993; Hacker and Wang, 1995; Zhang, 1997) and the paleomagnetic data showing clockwise rotation of the SCB relative to the NCB during the SCB–NCB collision resulting in a scissor-like suturing starting in the east and progressing west (Gilder and Courtillot, 1997) may not be supported by geo/thermochronology (this study; see Leech et al., 2006). The best estimates for UHP metamorphism in both Hong'an–Dabie and Sulu are based on U–Pb dating of coesite-bearing domains of zircon that show peak metamorphism occurred simultaneously in both areas: UHP zircon domains are dated at 244 ± 5–226 ± 2 Ma for Hong'an–Dabie and 243 ± 4–225 ± 2 Ma for Sulu. Prograde eclogite-facies(?) metamorphism may have begun as much as 10 Ma earlier in Hong'an–Dabie (c. 257 Ma) than in the Sulu area (c. 247 Ma).

Rotational exhumation models (e.g., Hacker et al., 2000) that require exhumation of UHP rocks in the eastern part of the orogen first may also not be supported by $^{40}Ar/^{39}Ar$ dating in Dabie and

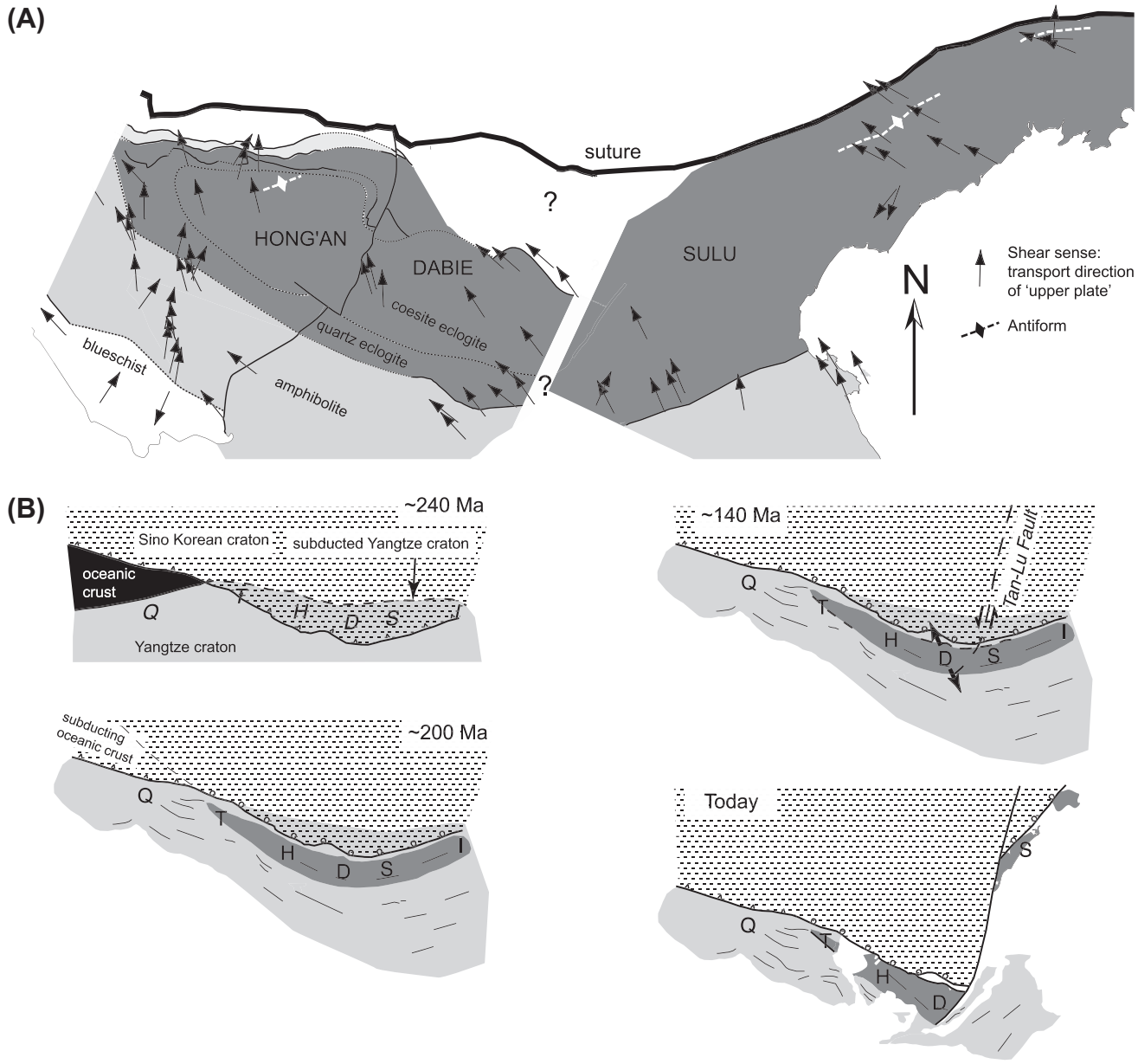

Fig. 5. (A) Pre-Cretaceous restoration modified after Hacker et al. (1998) with shear sense data associated with exhumation through amphibolite-to upper greenschist-facies conditions from Webb et al. (1999, 2006) and Hacker et al. (2000). Twenty-five degrees of counter-clockwise rotation of the Sulu terrane during Tan-Lu translation are required by the restoration. See text for further discussion. (B) Proposed evolution of the Hong'an–Dabie–Sulu orogen based on data reviewed here. Subduction of continental crust to UHP conditions is achieved by ~240 Ma. Exhumation of UHP rocks to or near upper-crustal depths is achieved by ~200 Ma. Sinistral offset along the Tan–Lu fault initiates by the Early Cretaceous and results in northward translation and rotation of the Sulu terrane relative to the Hong'an and Dabie Shan. Barbs and balls indicate upper plate of subduction and normal fault zones, respectively. Q = Qinling Shan, T = Tongbai Shan, H = Hong'an Shan, D = Dabie Shan, S = Sulu terrane, and I = Imjigang.

Sulu. Retrograde metamorphism began c. 220 Ma for both Hong'an–Dabie and Sulu, but retrograde zircon growth ended c. 214 Ma in Hong'an–Dabie and continued until c. 202 Ma in Sulu based on U–Pb dating of zircon domains external to coesite-bearing domains. The rotational exhumation model of Hacker et al. (2000) that shows a pivot point to the west of Hong'an–Dabie predicts greater exhumation in Sulu vs. Hong'an–Dabie, as well as later exhumation of Hong'an–Dabie UHP rocks relative to Sulu (c.f. Fig. 2 of Webb et al., 2008). Evaluating such trends and subtle differences between the relative timing of exhumation and final cooling across the orogen is complicated by the greater magnitude of Early Cretaceous extension (exhumation) and plutonism in the Dabie Shan compared to Hong'an and Sulu regions (Webb et al., 2006).

The best estimates for the initiation of sinistral motion on the Tan–Lu fault range from 143 to 120 Ma based on $^{40}Ar/^{39}Ar$ ages from mylonites in the southern part of the fault zone (Zhu et al., 2005). There is no significant body of evidence for pre-Cretaceous motion on the Tan–Lu fault, suggesting the fault did not play a role early in the history of SCB–NCB collision but that it developed later. However, these Cretaceous mylonite ages correspond to ages for widespread granitoids in both Dabie and Sulu, perhaps related to oblique subduction of the Pacific plate, similar to the model of Xu and Zhu (1994). Conversely, Early Cretaceous reactivation of the Tan–Lu fault may have reset ages on an older structure leaving open the possibility it formed earlier.

The structures in Sulu are broadly similar to those found in the Hong'an and Dabie Shan ~540 km to the south, further suggesting

the two areas have a common structural evolution that pre-dates motion on the Tan–Lu fault. To further assess this possibility, we constructed a pre-Cretaceous restoration of the Hong'an–Dabie–Sulu belt modified after Hacker et al. (1998) to include the Sulu region (Fig. 5). If the Tan–Lu fault initiated as a sinistral fault in the Early Cretaceous, it would have moved the Sulu terrane northward. By undoing this assumed translation and aligning the suture and the eclogite-facies isograd, the majority of the transport directions documented for the regions are also aligned. This restoration requires that the Sulu belt was rotated c. 25° counter-clockwise to achieve the current orientation of structures. We note that late- to post-collisional counter-clockwise rotation of the Sulu terrane relative to Hong'an–Dabie is consistent with the paleomagnetic studies of Gilder et al. (1999).

9. Conclusions

Our evaluation of published radiometric, paleomagnetic, and structural studies highlight the similarity of radiometric ages that constrain prograde, peak, and retrograde metamorphism in both regions, and the similar style and timing of tectonic exhumation in both regions. Additionally, c. 25° of counter-clockwise late- to post-collisional rotation of Sulu relative to Hong'an–Dabie required by our pre-Cretacous restoration is consistent with paleomagnetic data. The simplest conclusion supported by the data is that the Hong'an–Dabie–Sulu orogen is a piercing point for post-collisional offset on the Tan–Lu fault and that these regions shared a common subduction–exhumation history (Fig. 5B). We infer that the vast majority of left-lateral offset occurred in the Early Cretaceous, but do not discount the possible tectonic inheritance of the Tan–Lu fault as a transform fault with minor offset along a small circle about the NCB-SCB Euler pole.

Acknowledgements

We thank Alexander Robinson and one anonymous reviewer for their helpful suggestions for improving this manuscript.

Appendix A

Tables A1 and A2.

Table A1
Radiometric dating for the UHP unit of the Sulu area.

Age (Ma)	Error (±Ma)	Age type	Mineral	MSWD	Rock type	Reference
Ar/Ar						
222.2	2.4	WMA	Ph	6.8	Eclogite	Faure et al. (2003)
207.6	2.2	WMA	Ph	3.1	Gneiss	Faure et al. (2003)
205.0	3.2	Isochron	Amp	40.5	Amphibolite	Faure et al. (2003)
205.0	5.0	–	Bt	–	Gneiss	Faure et al. (2003)
196.4	2.0	Isochron	Bt	2.8	Gneiss	Faure et al. (2003)
121.9	1.4	Isochron	Bt	1.8	Gneiss	Faure et al. (2003)
279.6	1.4	Isochron	Ms	1.2	Orthogneiss	Hacker et al. (2009)
215.8	1.7	Isochron	Bt	0.0	Schist	Hacker et al. (2009)
209.7	1.1	WMPA	Bt	0.4	Gneiss	Hacker et al. (2009)
207.0	1.8	WMPA	Bt	–	Orthogneiss	Hacker et al. (2009)
197.4	8.0	Isochron	Ms	3.1	Granite	Hacker et al. (2009)
157.8	4.6	WMPA	Bt	3.4	Gneiss	Hacker et al. (2009)
150.7	0.8	WMPA	Bt	1.0	Gneiss	Hacker et al. (2009)
141.2	3.6	Isochron	Hbl	3.5	Amphibolite	Hacker et al. (2009)
124.7	1.1	WMA	Bt	–	Orthogneiss	Hacker et al. (2009)
115.7	4.4	WMPA	Bt	0.2	Granite	Hacker et al. (2009)
100.0	0.7	TFA	Bt	–	Granite	Hacker et al. (2009)
67.6	2.4	WMPA	Bt	0.7	Orthogneiss	Hacker et al. (2009)
209.0	0.7	WMPA	Amp	1.3	Amphibolite	Liu et al. (2008)
207.0	0.7	WMPA	Amp	1.3	Amphibolite	Liu et al. (2008)
215.0	0.5	WMPA	Bt	0.7	Paragneiss	Liu et al. (2009b)
212.0	0.7	WMPA	Bt	1.5	Paragneiss	Liu et al. (2009b)
203.0	0.6	WMPA	Bt	1.1	Paragneiss	Liu et al. (2009b)
201.0	0.6	WMPA	Bt	0.5	Paragneiss	Liu et al. (2009b)
213.5	1.4	WMA	WM	11.1	Schist	Webb et al. (2006)
213.4	1.2	WMA	Bt	7.1	Shear band	Webb et al. (2006)
212.9	1.3	WMA	Amp	7.5	Orthogneiss	Webb et al. (2006)
206.6	1.0	WMA	Bt	6.6	Orthogneiss	Webb et al. (2006)
206.1	1.3	WMA	Kfs	–	Orthogneiss	Webb et al. (2006)
159.9	0.6	WMA	WM	2.7	Mylonite	Webb et al. (2006)
145.3	6.6	WMA	WM	14.0	Mylonite	Webb et al. (2006)
135.6	0.5	WMA	Bt	3.3	L–S tectonite	Webb et al. (2006)
69.6	2.5	WMA	Bt	12.0	Orthogneiss	Webb et al. (2006)
Rb–Sr						
223.9	0.9	Ms, WR	–	–	Eclogite	Li et al. (1994)
219.5	0.5	Ms, WR	–	–	Eclogite	Li et al. (1994)
224.0	2.0	Min-WR isochron	3	–	Eclogite	Li et al. (1999)
219.0	2.0	Min-WR isochron	3	–	Eclogite	Li et al. (1999)
216.0	31.0	Cpx, Ph, WR	–	17.0	Eclogite	Zhao et al. (2006b)
216.0	6.0	Cpx, Ph, WR	–	0.0	Eclogite	Zhao et al. (2006b)
Sm–Nd						
214.0	10.0	Min-WR isochron	–	1.4	Orthogneiss	Gong et al. (2007)
221.0	6.0	Min isochron	2	–	Eclogite	Li et al. (1993)
209.0	31.0	Min isochron	4	–	Eclogite	Li et al. (1993)

(*continued on next page*)

Table A1 (*continued*)

Age (Ma)	Error (±Ma)	Age type	Mineral	MSWD	Rock type	Reference
228.4	6.0	Grt, Cpx, WR	–	–	Eclogite	Li et al. (1994)
226.3	4.5	Grt, Cpx, WR	–	–	Eclogite	Li et al. (1994)
228.0	6.0	Isochron	–	–	–	Li et al. (1999)
226.3	4.5	Min-WR isochron	4	0.9	Eclogite	Li et al. (1999)
220.6	7.1	Grt, Cpx, WR	3	1.3	Eclogite	Schmidt et al. (2008)
216.0	10.0	Grt, Cpx, WR	–	0.4	Eclogite	Zhao et al. (2006b)
215.0	9.0	Grt, Cpx, Rt, WR	–	0.7	Eclogite	Zhao et al. (2006b)
226.0	5.0	Min-WR isochron	4	–	Eclogite	Zheng et al. (2002)
221.0	18.0	Min isochron	2	–	Eclogite	Zheng et al. (2002)
211.0	6.0	Min isochron	2	–	Eclogite	Zheng et al. (2002)
208.0	15.0	Min isochron	2	–	Eclogite	Zheng et al. (2002)
Lu–Hf						
222.7	1.6	Grt, Cpx isochron	3	0.2	Eclogite	Schmidt et al. (2008)
221.4	1.2	Grt, Cpx isochron	3	0.8	Eclogite	Schmidt et al. (2008)
219.6	1.4	Grt, Cpx isochron	2	–	Eclogite	Schmidt et al. (2008)
221.6	1.7	Grt, Cpx, Zrn isochron	7	1.8	Eclogite	Schmidt et al. (2011)
220.5	2.7	Grt, Cpx isochron	4	1.8	Eclogite	Schmidt et al. (2011)
218.0	1.7	Grt, Cpx isochron	3	1.3	Eclogite	Schmidt et al. (2011)
217.8	1.2	Grt, Cpx isochron	3	0.02	Eclogite	Schmidt et al. (2011)
215.9	1.3	Grt, Cpx isochron	4	0.03	Eclogite	Schmidt et al. (2011)
215.8	0.9	Grt, Cpx isochron	4	2.8	Eclogite	Schmidt et al. (2011)

Age (Ma)	Error (±Ma)	Method	Age type	Number of analyses	MSWD	Rock type	Reference
U–Pb							
217.1	8.7	Conv	LIA	6	–	Eclogite	Ames et al. (1996)
177.0	45.0	Conv	LIA	–	–	Gneiss	Ames et al. (1996)
220.0	7.0	IMP	WMA	7	1.3	Eclogite	Chen et al. (2011)
218.0	2.0	IMP	WMA	10	0.4	Granitic gneiss	Chen et al. (2011)
219.0	3.0	IMP	WMA	14	2.4	Granitic gneiss	Chen et al. (2011)
220.0	4.0	IMP	WMA	11	2.2	Granitic gneiss	Chen et al. (2011)
240.0	7.0	LA-ICPMS	WMA	11	0.0	Eclogite	Gao et al. (2010)
226.0	2.0	LA-ICPMS	WMA	12	0.0	Eclogite	Gao et al. (2010)
213.9	4.9	LA-ICPMS	WMA	11	0.7	Eclogite	Gao et al. (2010)
214.0	9.0	LA-ICPMS	LIA	–	0.8	Orthogneiss	Gong et al. (2007)
226.0	4.6	IMP-ICPMS	WMA	2	2.3	Granitic gneiss	Hacker et al. (2006)
223.7	4.9	IMP-ICPMS	WMA	2	0.1	Augen gneiss	Hacker et al. (2006)
218.7	2.2	IMP-ICPMS	WMA	8	0.7	Granitic gneiss	Hacker et al. (2006)
229.5	5.6	IMP-ICPMS	WMA	15	0.5	Granitic gneiss	Hacker et al. (2006)
216.3	2.4	IMP-ICPMS	WMA	6	0.2	Granitic gneiss	Hacker et al. (2006)
204.7	2.6	IMP-ICPMS	WMA	8	–	Granitic gneiss	Hacker et al. (2006)
202.4	2.7	IMP-ICPMS	WMA	6	0.2	Granitic gneiss	Hacker et al. (2006)
232.0	2.0	SHRIMP	SG	1	–	Orthogneiss	Leech et al. (2006)
222.0	3.0	SHRIMP	SG	1	–	Orthogneiss	Leech et al. (2006)
219.0	1.0	SHRIMP	WMA	8	0.1	Orthogneiss	Leech et al. (2006)
215.0	2.0	SHRIMP	SG	1	–	Orthogneiss	Leech et al. (2006)
215.0	6.0	SHRIMP	WMA	18	0.5	Orthogneiss	Leech et al. (2006)
214.0	4.0	SHRIMP	WMA	4	0.0	Orthogneiss	Leech et al. (2006)
211.0	2.0	SHRIMP	WMA	3	0.1	Orthogneiss	Leech et al. (2006)
208.0	3.0	SHRIMP	WMA	2	0.7	Orthogneiss	Leech et al. (2006)
207.0	3.0	SHRIMP	WMA	5	0.1	Orthogneiss	Leech et al. (2006)
202.0	13.0	Conv	LIA	–	–	–	Li et al. (1999)
232.0	6.2	SHRIMP	WMA*	2	0.6	Quartzite	Liu and Liou (2011)
230.6	6.2	SHRIMP	WMA*	2	0.4	Gneiss	Liu and Liou (2011)
229.0	4.2	SHRIMP	WMA*	2	0.9	Eclogite	Liu and Liou (2011)
228.6	3.2	SHRIMP	WMA*	3	0.2	Gneiss	Liu and Liou (2011)
228.6	4.3	SHRIMP	WMA*	3	0.0	Gneiss	Liu and Liou (2011)
225.5	4.1	SHRIMP	WMA*	4	0.2	Gneiss	Liu and Liou (2011)
215.0	4.0	SHRIMP	SG	–	–	Gneiss	Liu and Liou (2011)
215.0	5.0	SHRIMP	SG	–	–	Gneiss	Liu and Liou (2011)
214.0	3.0	SHRIMP	SG	–	–	Quartzite	Liu and Liou (2011)
212.4	6.2	SHRIMP	WMA*	2	0.0	Eclogite	Liu and Liou (2011)
210.8	6.2	SHRIMP	WMA*	2	0.1	Gneiss	Liu and Liou (2011)
204.6	4.8	SHRIMP	WMA*	2	0.6	Gneiss	Liu and Liou (2011)
233.7	4.4	SHRIMP	WMA	8	0.1	Eclogite & gneiss	Liu and Xu (2004)
213.2	5.2	SHRIMP	WMA	3	0.3	Gneiss	Liu and Xu (2004)
232.0	4.0	IMP	WMA	16	1.8	Gneiss	Liu et al. (2004a)
228.0	5.0	IMP	WMA	14	1.1	Gneiss	Liu et al. (2004a)
213.0	5.0	IMP	WMA	6	1.7	Gneiss	Liu et al. (2004a)
208.0	4.0	IMP	WMA	6	2.2	Gneiss	Liu et al. (2004a)
227.3	2.1	IMP	WMA*	17	1.0	Granitic gneiss	Liu et al. (2004b)
208.7	2.7	IMP	WMA*	12	0.8	Granitic gneiss	Liu et al. (2004b)
227.0	9.0	SHRIMP	WMA	10	0.2	Gneiss	Liu et al. (2005)
244.8	2.8	SHRIMP	WMA	11	–	Eclogite	Liu et al. (2006a)

Table A1 (*continued*)

Age (Ma)	Error (±Ma)	Method	Age type	Number of analyses	MSWD	Rock type	Reference
243.1	1.4	SHRIMP	WMA	6	–	Eclogite	Liu et al. (2006a)
242.0	2.9	SHRIMP	WMA	12	–	Eclogite	Liu et al. (2006a)
240.5	4.7	SHRIMP	WMA	3	–	Eclogite	Liu et al. (2006a)
227.6	3.7	SHRIMP	WMA	4	–	Eclogite	Liu et al. (2006a)
227.0	2.6	SHRIMP	WMA	15	–	Eclogite	Liu et al. (2006a)
224.8	2.7	SHRIMP	WMA	9	–	Eclogite	Liu et al. (2006a)
246.9	3.9	SHRIMP	WMA*	9	0.3	Marble	Liu et al. (2006b)
233.6	2.7	SHRIMP	WMA*	12	0.1	Marble	Liu et al. (2006b)
212.9	6.0	SHRIMP	WMA*	4	0.5	Marble	Liu et al. (2006b)
225.6	4.8	SHRIMP	WMA*	17	0.2	Orthogneiss	Liu et al. (2006c)
214.3	5.2	SHRIMP	WMA*	12	0.2	Orthogneiss	Liu et al. (2006c)
210.3	2.5	SHRIMP	WMA*	11	1.0	Orthogneiss	Liu et al. (2006c)
244.0	4.0	SHRIMP	WMA	16	0.8	Eclogite	Liu et al. (2007)
233.0	4.0	SHRIMP	WMA	12	2.4	Eclogite	Liu et al. (2007)
214.0	5.0	SHRIMP	WMA	8	0.8	Eclogite	Liu et al. (2007)
231.0	4.0	SHRIMP	WMA	12	1.6	Amphibolite	Liu et al. (2008)
231.0	3.0	SHRIMP	WMA	10	1.4	Amphibolite	Liu et al. (2008)
215.0	3.0	SHRIMP	WMA	9	1.9	Amphibolite	Liu et al. (2008)
214.0	4.0	SHRIMP	WMA	10	1.8	Amphibolite	Liu et al. (2008)
230.0	7.0	SHRIMP	WMA	11	1.2	Paragneiss	Liu et al. (2009a)
230.0	7.0	SHRIMP	WMA	11	1.2	Orthogneiss	Liu et al. (2009a)
210.0	2.0	SHRIMP	WMA	9	0.9	Paragneiss	Liu et al. (2009a)
210.0	3.0	SHRIMP	WMA	8	0.9	Orthogneiss	Liu et al. (2009a)
228.0	2.0	SHRIMP	WMA	11	1.2	Orthogneiss	Liu et al. (2009b)
228.0	3.0	SHRIMP	WMA	11	1.3	Orthogneiss	Liu et al. (2009b)
218.0	2.0	SHRIMP	WMA	11	1.5	Orthogneiss	Liu et al. (2009b)
218.0	3.0	SHRIMP	WMA	11	1.4	Orthogneiss	Liu et al. (2009b)
217.0	3.0	SHRIMP	WMA	12	1.1	Orthogneiss	Liu et al. (2009b)
217.0	4.0	SHRIMP	WMA	10	0.9	Orthogneiss	Liu et al. (2009b)
215.0	3.0	SHRIMP	WMA	9	0.9	Orthogneiss	Liu et al. (2009b)
215.0	2.0	SHRIMP	WMA	9	1.6	Orthogneiss	Liu et al. (2009b)
202.0	2.0	SHRIMP	WMA	8	0.8	Orthogneiss	Liu et al. (2009b)
202.0	4.0	SHRIMP	WMA	9	1.3	Orthogneiss	Liu et al. (2009b)
202.0	2.0	SHRIMP	WMA	9	1.8	Orthogneiss	Liu et al. (2009b)
202.0	2.0	SHRIMP	WMA	8	0.9	Orthogneiss	Liu et al. (2009b)
233.1	5.3	LA-ICPMS	WMA	14	–	Eclogite	Riemann et al. (2010)
207.4	1.6	LA-ICPMS	WMA	21	–	Eclogite	Riemann et al. (2010)
233.0	2.0	IMP	SG	1	–	Garnet peridotite	Rumble et al. (2002)
223.0	2.0	IMP	SG	1	–	Gneiss	Rumble et al. (2002)
220.0	1.0	IMP	WMA	2	0.6	Garnet peridotite	Rumble et al. (2002)
217.0	2.0	–	LIA	–	–	Eclogite	Schmidt et al. (2011)
217.0	2.0	–	LIA	–	–	Eclogite	Schmidt et al. (2011)
239.0	7.0	SHRIMP	SG	1	–	Eclogite	Tang et al. (2008)
235.0	3.0	LA-ICPMS	WMA	13	0.4	Orthogneiss	Tang et al. (2008)
234.0	3.0	LA-ICPMS	WMA	5	0.3	Orthogneiss	Tang et al. (2008)
229.0	3.0	LA-ICPMS	WMA	16	1.5	Eclogite	Tang et al. (2008)
227.0	3.0	LA-ICPMS	SG	1	–	Orthogneiss	Tang et al. (2008)
217.0	22.0	LA-ICPMS	WMA	3	5.8	Orthogneiss	Tang et al. (2008)
222.0	2.0	IMP	WMA#	14	1.3	Dike	Wallis et al. (2005)
207.0	1.0	IMP	WMA#	11	0.8	Dike	Wallis et al. (2005)
223.0	4.0	LA-ICPMS	WMA	18	2.2	Quartzite	Wang et al. (2011)
221.0	4.0	LA-ICPMS	WMA	20	2.2	Quartzite	Wang et al. (2011)
228.0	29.0	IMP	LIA	24	1.3	Eclogite	Yang et al. (2003)
221.0	12.0	IMP	Prob curve	9	47.0	Peridotite	Yang et al. (2003)
231.0	5.0	LA-ICPMS	WMA	8	6.0	Marble	Yu et al. (2011)
201.0	4.0	LA-ICPMS	SG	1	–	Quartzite	Yu et al. (2011)
217.0	3.0	LA-ICPMS	SG	1	–	Quartzite	Yu et al. (2011)
212.0	3.0	LA-ICPMS	SG	1	–	Quartzite	Yu et al. (2011)
219.0	4.0	LA-ICPMS	SG	1	–	Quartzite	Yu et al. (2011)
235.0	7.0	IMP	WMA*	20	114.0	Eclogite	Zhao et al. (2005)
242.0	6.0	IMP	WMA*	10	18.0	Eclogite	Zhao et al. (2005)
242.0	8.0	SHRIMP	WMA	3	0.3	Dunite	Zhao et al. (2006a)
238.0	3.0	SHRIMP	WMA	10	1.5	Eclogite	Zhao et al. (2006a)
232.0	7.0	SHRIMP	WMA	7	1.3	Eclogite	Zhao et al. (2006a)
218.0	5.0	SHRIMP	WMA	19	1.6	Eclogite	Zhao et al. (2006a)
216.0	3.0	SHRIMP	WMA	10	1.5	Eclogite	Zhao et al. (2006b)
215.0	2.0	SHRIMP	WMA	11	3.9	Garnet peridotite	Zhao et al. (2007a)
225.0	2.0	SHRIMP	WMA	14	1.1	Eclogite	Zhao et al. (2007b)
258.0	25.0	IMP	SG	1	–	Eclogite	Zheng et al. (2004)
247.0	5.0	IMP	SG	1	–	Eclogite	Zheng et al. (2004)
241.0	5.0	IMP	SG	1	–	Eclogite	Zheng et al. (2004)
231.0	7.0	IMP	SG	1	–	Eclogite	Zheng et al. (2004)
229.0	7.0	IMP	SG	1	–	Eclogite	Zheng et al. (2004)
227.0	3.0	IMP	SG	1	–	Granitic gneiss	Zheng et al. (2004)
226.0	7.0	IMP	SG	1	–	Eclogite	Zheng et al. (2004)

(*continued on next page*)

Table A1 (*continued*)

Age (Ma)	Error (±Ma)	Method	Age type	Number of analyses	MSWD	Rock type	Reference
224.0	14.0	Conv	LIA	5	4.0	Granitic gneiss	Zheng et al. (2004)
224.0	27.0	Conv	LIA	6	7.9	Granitic gneiss	Zheng et al. (2004)
219.0	8.0	IMP	SG	1	–	Eclogite	Zheng et al. (2004)
218.0	16.0	Conv	LIA	5	6.5	Granitic gneiss	Zheng et al. (2004)
217.0	3.0	IMP	SG	1	–	Eclogite	Zheng et al. (2004)
215.0	6.0	IMP	SG	1	–	Eclogite	Zheng et al. (2004)
221.0	6.0	LA-ICPMS	WMA	–	3.9	Eclogite	Zheng (2009)
230.0	4.0	LA-ICPMS	WMA	13	1.1	Eclogite	Zong et al. (2009)
229.0	5.0	LA-ICPMS	WMA	11	0.5	Eclogite	Zong et al. (2009)
210.0	4.0	LA-ICPMS	WMA	11	11.0	Eclogite	Zong et al. (2009)
209.0	4.0	LA-ICPMS	WMA	11	10.3	Eclogite	Zong et al. (2009)

Notes: Notation for type of ages: Conv, conventional isotope dilution; IMP, ion microprobe analysis; IMP-ICPMS, combination of ion microprobe and ICP-MS U–Pb analyses; Isochron, isochron age for either Sm–Nd or Rb–Sr dating (min, mineral; WR, whole-rock) or inverse isochron age for $^{40}Ar/^{39}Ar$ data; LA-ICPMS, laser ablation ICPMS; LIA, lower intercept age on concordia diagram; prob curve, peak on probability density curve; SG, single-grain, either age from a single grain or single spot age from ion microprobe analysis; SHRIMP, sensitive high resolution ion microprobe; TFA-LF, total fusion age-laser fuison; WMA, weighted mean age of multiple analyses; WMA*, weighted mean age recalculated from original publication; WMPA, weighted mean plateau age. Missing data indicates data not reported in original publication. When omitted from original publication and when possible from published data, MSWD was calculated from original data; the number of analyses were calculated or estimated from original data when not explicitly stated in original publication. Errors reported are 1σ. MSWD, mean square of weighted deviates. Mineral abbreviations (from Whitney and Evans, 2010): Amp, amphibole; Bt, biotite, Grt, garnet; Hbl, hornblende; Kfs, K-feldspar; Mnz, monazite; Ms, muscovite; Pg, paragonite; Ph, phengite; Pl, plagioclase; Cpx, clinopyroxene; WM, white mica. UM, ultramafic. Samples with very large errors were excluded; zircon ages with prograde inclusions were excluded (e.g., Liu et al., 2006). # Weighted mean age calculated for individual analyses reported in Wallis et al. (2005).

Table A2
Radiometric dating for the UHP units of the Hong'an–Dabie area.

Age (Ma)	Error (±Ma)	Age type	Mineral	MSWD	Rock type	Reference
Ar/Ar						
230.1	0.4	TFPA	Ph	–	Gneiss	Eide et al. (1994)
195.2	0.2	TFPA	Ph	–	Gneiss	Eide et al. (1994)
124.8	1.2	WMA	Ms	2.3	Granite	Grimmer et al. (2002)
119.9	0.3	TFA	Kfs	–	Syenite	Grimmer et al. (2002)
103.7	0.3	WMA	Bt	1.7	Orthogneiss	Grimmer et al. (2002)
90.5	0.2	TFA	Kfs	–	Granite	Grimmer et al. (2002)
228.7	0.7	WMPA	Bt	2.4	Paragneiss	Hacker and Wang (1995)
206.0	0.6	WMPA	Ph	0.3	Paragneiss	Hacker and Wang (1995)
199.7	1.0	WMPA	Ph	0.1	Paragneiss	Hacker and Wang (1995)
190.2	0.6	WMPA	Bt	3.9	Paragneiss	Hacker and Wang (1995)
188.6	0.6	WMPA	Ph	1.5	Paragneiss	Hacker and Wang (1995)
178.3	0.9	WMPA	Ph	0.9	Paragneiss	Hacker and Wang (1995)
241.9	2.3	TFA	Ms	–	–	Hacker et al. (2000)
216.0	2.0	WMPA	Bt	0.5	–	Hacker et al. (2000)
199.3	1.9	WMA	Bt	–	–	Hacker et al. (2000)
195.2	1.8	WMPA	Bt	1.0	–	Hacker et al. (2000)
194.6	1.8	WMPA	Ms	1.0	–	Hacker et al. (2000)
183.3	1.7	TFA	Ms	–	–	Hacker et al. (2000)
177.0	1.0	–	–	–	Orthogneiss	Li and Lo (1999), cit. in Li et al. (1999)
170.0	1.0	–	–	–	Orthogneiss	Li and Lo (1999), cit. in Li et al. (1999)
231.0	5.0	K–Ar	Bt	–	Gneiss	Li et al. (1993)
241.3	3.1	WMPA	Pg	0.1	Eclogite	Li et al. (2004)
244.3	1.8	WMPA	Ph	–	Eclogite	Okay et al. (1993)
264.6	3.2	WMPA	Ph	0.3	Eclogite	Qiu et al. (2010)
242.2	2.3	WMPA	Hbl	6.2	Vein	Qiu et al. (2010)
223.3	4.2	WMPA	Pg	0.6	Eclogite	Qiu et al. (2010)
217.6	4.8	WMPA	Hbl	0.1	Eclogite	Qiu et al. (2010)
217.3	1.8	WMPA	Pg	0.9	Eclogite	Qiu et al. (2010)
217.0	2.9	WMPA	Pg	3.2	Eclogite	Qiu et al. (2010)
204.0	4.8	WMPA	Pg	2.8	Vein	Qiu et al. (2010)
203.2	4.4	WMPA	Pg	5.1	Eclogite	Qiu et al. (2010)
200.9	3.1	WMPA	Hbl	0.3	Vein	Qiu et al. (2010)
199.4	3.3	WMPA	Pg	2.5	Eclogite	Qiu et al. (2010)
130.0	1.3	TFA	Ms	–	Paragneiss	Ratschbacher et al. (2000)
131.0	2.0	WMA	Bt	–	Paragneiss	Ratschbacher et al. (2000)
194.7	1.9	TFA	Hbl	–	Amphibolite	Ratschbacher et al. (2000)
117.5	1.1	WMA	Bt	–	Gabbro	Ratschbacher et al. (2000)
122.0	2.0	WMA	Hbl	–	Gabbro	Ratschbacher et al. (2000)
120.3	3.4	TFA	Kfs	–	–	Ratschbacher et al. (2006)
106.5	3.1	TFA	Kfs	–	–	Ratschbacher et al. (2006)
118.1	1.1	TFA	Kfs	–	–	Ratschbacher et al. (2006)
234.9	2.5	WMA	Ms	0.7	–	Ratschbacher et al. (2006)
214.5	0.6	–	Ms	1.9	–	Ratschbacher et al. (2006)
234.0	1.0	WMA	WM	–	Eclogite	Webb et al. (1999, 2001)
234.0	2.0	WMA	WM	–	Mylonite	Webb et al. (1999, 2001)

Table A2 (*continued*)

Age (Ma)	Error (±Ma)	Age type	Mineral	MSWD	Rock type	Reference
233.0	2.0	WMA	WM	–	Shear band	Webb et al. (1999, 2001)
231.0	2.0	WMA	WM	–	Shear band	Webb et al. (1999, 2001)
224.0	2.0	WMA	WM	–	Shear band	Webb et al. (1999, 2001)
222.0	2.0	WMA	WM	–	Eclogite	Webb et al. (1999, 2001)
206.0	2.0	WMA	WM	–	Gneiss	Webb et al. (1999, 2001)
196.0	2.0	WMA	WM	–	Gneiss	Webb et al. (1999, 2001)
Rb–Sr						
223.0	13.0	Min-WR isochron	3	7.4	Eclogite	Chavagnac and Jahn (1996)
214.0	6.0	Min-WR isochron	3	2.0	Eclogite	Chavagnac and Jahn (1996)
212.0	5.0	Min-WR isochron	2	–	Eclogite	Chavagnac and Jahn (1996)
212.0	19.0	Min isochron	4	2.5	–	Chavagnac and Jahn (1996)
134.4	0.5	Isochron	–	–	Retrograded eclogite	Li et al., 1993
223.0	13.0	Min-WR isochron	3	–	Eclogite	Li et al. (1999)
214.0	6.0	Min-WR isochron	4	–	Eclogite	Li et al. (1999)
230.0	7.0	Min isochron	3	1.9	Eclogite	Li et al. (2004)
212.0	7.0	Min-WR isochron	5	16.0	Eclogite	Liu et al. (2004)c
240.0	2.0	Min-WR isochron	2	–	Eclogite	Okay et al. (1993)
236.0	3.0	Min-WR isochron	2	–	Eclogite	Okay et al. (1993)
231.0	48.0	Ms, Pl, WR	–	–	Amphibolite	Sang et al. (1987), cit. in Hacker et al. (1996)
Sm–Nd						
225.0	7.0	Min isochron	7	0.7	Garnets	Chavagnac and Jahn (1996)
218.0	4.0	Min isochron	2	–	Eclogite	Chavagnac and Jahn (1996)
215.0	5.0	Min-WR isochron	3	0.5	Eclogite	Chavagnac and Jahn (1996)
214.0	7.0	Min-WR isochron	3	0.4	Eclogite	Chavagnac and Jahn (1996)
213.0	3.0	Min-WR isochron	2	–	Eclogite	Chavagnac and Jahn (1996)
211.0	4.0	Min-WR isochron	3	0.6	Eclogite	Chavagnac and Jahn (1996)
210.0	9.0	Min-WR isochron	3	0.3	Eclogite	Chavagnac and Jahn (1996)
210.0	7.0	Min-WR isochron	3	0.0	Peridotite	Chavagnac and Jahn (1996)
238.0	10.0	–	–	–	Eclogite	Chen et al. (1998), cit. in Ratschbacher et al. (2006)
224.2	2.1	Grt, Cpx, WR	6	0.5	Eclogite	Cheng et al. (2008)
222.5	5.0	Ky, Grt, Cpx, WR	4	3.7	Eclogite	Cheng et al. (2008)
217.8	6.1	Ky, Grt, Cpx, WR	5	9.3	Eclogite	Cheng et al., 2008
244.0	11.0	–	–	–	Garnet pyroxenite	Li et al. (1989), cit. in Ratschbacher et al. (2006)
244.0	11.0	Min-WR isochron	3	–	Eclogite, UM?	Li et al. (1993)
229.0	3.0	Min-WR isochron	4	–	Grt-Bt Gneiss	Li et al. (1993)
224.0	20.0	Min isochron	3	–	Eclogite	Li et al. (1993)
221.0	5.0	Min isochron	4	–	Eclogite	Li et al. (1993)
226.2	2.9	Min-WR isochron	4	0.3	Eclogite	Li et al. (1999)
226.5	2.8	Min-WR isochron	6	0.1	Gneiss	Li et al. (1999)
236.0	4.0	Min isochron	4	1.4	–	Li et al. (2004)
230.0	6.0	–	–	–	Eclogite	Liu et al. (2000), cit. in Ratschbacher et al. (2006)
226.0	6.0	–	–	–	Banded Gneiss	Liu et al. (2000), cit. in Ratschbacher et al. (2006)
210.0	6.0	–	–	–	Eclogite	Liu et al. (2000), cit. in Ratschbacher et al. (2006)
208.0	38.0	–	–	–	Eclogite	Liu et al., 2001, cit. in Ratschbacher et al., 2006
208.0	4.0	–	–	–	Eclogite	Liu et al. (2000), cit. in Ratschbacher et al. (2006)
246.0	8.0	Min-WR isochron	2	–	Eclogite	Okay et al. (1993)
222.1	7.2	Grt, Cpx, WR	3	0.2	Eclogite	Schmidt et al. (2008)
229.0	18.0	LIA	–	–	Banded Gneiss	Xie et al. (2001), cit. in Ratschbacher et al. (2006)
229.0	13.0	–	–	–	Eclogite?	Xie et al. (2004)
219.0	11.0	–	–	–	Eclogite?	Xie et al. (2004)
Lu–Hf						
240.0	5.0	Ky, Grt, Cpx, WR	3	2.6	Eclogite	Cheng et al. (2008)
230.8	5.0	Grt, Cpx, WR	6	3.7	Eclogite	Cheng et al. (2008)
224.4	1.9	Ky, Grt, WR	6	1.7	Eclogite	Cheng et al. (2008)
242.2	2.6	Grt, WR	5	0.3	Eclogite	Cheng et al. (2011)
223.4	0.9	Grt, Cpx	3	0.1	Eclogite	Schmidt et al. (2008)
222.9	0.9	Grt, Cpx	3	2.2	Eclogite	Schmidt et al. (2008)

Age (Ma)	Error (±Ma)	Method	Age type	Number of analyses	MSWD	Rock type	Reference
U–Pb							
212.0	11.0	Conv	LIA	4	–	Eclogite	Ames et al. (1993)
209.0	2.0	Conv	LIA	3	–	Eclogite	Ames et al. (1993)
227.0	22.0	Conv	LIA	4	–	Gneiss	Ames et al. (1996)
218.5	1.8	Conv	LIA	3	–	Eclogite	Ames et al. (1996)
218.4	2.5	Conv	LIA	3	–	Eclogite	Ames et al. (1996)
214.2	9.6	Conv	LIA	3	–	Eclogite	Ames et al. (1996)
135.0	42.0	Conv	LIA	–	–	Eclogite	Ames et al. (1996)
238.0	3.0	IMP	WMA	6	0.7	Quartzite	Ayers et al. (2002)
236.0	32.0	IMP	LIA	11	7.0	Quartzite	Ayers et al. (2002)
230.6	2.8	IMP	WMA	26	0.7	Eclogite	Ayers et al. (2002)
223.0	1.0	Pb-Th IMP	LIA	6	–	Quartzite	Ayers et al. (2002)
209.2	1.8	Pb-Th IMP	Isochron	25	0.7	Clinopyroxenite	Ayers et al. (2002)
223.0	8.0	LA-ICPMS	WMA	14	38.0	Eclogite	Cheng et al. (2011)

(*continued on next page*)

Table A2 (*continued*)

Age (Ma)	Error (±Ma)	Method	Age type	Number of analyses	MSWD	Rock type	Reference
262.0	3.0	SHRIMP		–	–	Eclogite	Gao et al. (2002), cit. in Ratschbacher et al. (2006)
242.0	2.0	LA-ICPMS	WMA	10	1.6	Eclogite	Gao et al. (2011)
226.0	2.0	LA-ICPMS	WMA	10	1.9	Eclogite	Gao et al. (2011)
239.0	29.0	LA-ICPMS	LIA	4	2.1	Eclogite	Gao et al. (2011)
241.0	3.0	LA-ICPMS	WMA	3	0.5	Eclogite	Gao et al. (2011)
224.0	5.0	LA-ICPMS	SG	1	–	Eclogite	Gao et al. (2011)
236.0	3.0	IMP	Prob curve	12	–	Gneiss	Hacker et al. (1998)
225.0	4.0	IMP	Prob curve	8	–	Gneiss	Hacker et al. (1998)
238.4	1.3	Conv	SG	–	–	–	Li et al. (1999)
236.2	2.4	Conv	SG	–	–	–	Li et al. (1999)
254.0	30.0	IMP	LIA	7	2.9	Eclogite	Li et al. (2004)
242.0	3.0	IMP	WMA	8	2.1	Eclogite	Li et al. (2004)
222.0	4.0	IMP	WMA	3	0.1	Eclogite	Li et al. (2004)
243.0	1.0	–	–	–	–	Jadeite Quartzite	Liu and Jahn (2004), cit. in Wu et al. (2006)
228.0	2.0	–	–	–	–	Jadeite Quartzite	Liu and Jahn (2004), cit. in Wu et al. (2006)
243.0	9.1	SHRIMP	WMA*	2	0.2	Eclogite	Liu and Liou (2011)
234.1	8.1	SHRIMP	WMA*	3	0.0	Eclogite	Liu and Liou (2011)
217.0	6.0	SHRIMP	SG	–	–	Eclogite	Liu and Liou (2011)
213.0	5.0	IMP	WMA	13	–	Eclogite	Liu et al. (2004c)
242.5	0.5	SHRIMP	WMA	23	–	Jadeite Quartzite	Liu et al. (2006a)
241.4	1.6	SHRIMP	WMA	15	–	Garnet pyroxenite	Liu et al., 2006a
240.8	0.9	SHRIMP	WMA	16	–	Eclogite	Liu et al. (2006a)
227.9	2.8	SHRIMP	WMA	–	–	Eclogite	Liu et al. (2006a)
227.4	1.1	SHRIMP	WMA	8	–	Jadeite Quartzite	Liu et al. (2006a)
227.3	1.5	SHRIMP	WMA	14	–	Garnet pyroxenite	Liu et al. (2006a)
226.7	2.6	SHRIMP	WMA	15	–	Garnet peridotite	Liu et al. (2006a)
220.4	1.3	SHRIMP	WMA	22	–	Eclogite	Liu et al. (2006a)
220.1	2.3	SHRIMP	WMA	–	–	Eclogite	Liu et al. (2006a)
219.3	1.1	SHRIMP	WMA	–	–	Garnet Gneiss	Liu et al. (2006a)
243.8	3.8	SHRIMP	WMA*	10	0.6	Marble	Liu et al. (2006b)
233.0	2.8	SHRIMP	WMA*	13	0.3	Marble	Liu et al. (2006b)
214.4	5.4	SHRIMP	WMA*	5	0.5	Marble	Liu et al. (2006b)
245.0	4.0	SHRIMP	WMA	13	1.4	Eclogite	Liu et al. (2007)
235.0	3.0	SHRIMP	WMA	15	1.2	Eclogite	Liu et al. (2007)
215.0	6.0	SHRIMP	WMA	10	2.9	Eclogite	Liu et al. (2007)
229.0	8.0	LA-ICPMS	LIA		2.9	Eclogite	Liu et al. (2011)
227.0	2.0	SHRIMP	WMA	15	1.6	Eclogite	Liu et al. (2011)
226.0	3.0	LA-ICPMS	WMA	13	0.6	Eclogite	Liu et al. (2011)
222.0	4.0	SHRIMP	WMA	4	0.3	Eclogite	Liu et al. (2011)
215.0	2.0	SHRIMP	WMA	14	0.8	Eclogite	Liu et al. (2011)
213.0	3.0	LA-ICPMS	WMA	9	0.9	Eclogite	Liu et al. (2011)
210.0	4.0	SHRIMP	WMA	4	0.2	Eclogite	Liu et al. (2011)
224.0	9.0	SHRIMP	–	–	–	–	Maruyama et al. (1998), cit. in Hacker and Wang (1995)
225.5	3.0	Conv	LIA	6	–	Eclogite	Rowley et al. (1997)
218.5	1.7	Conv	LIA	15	–	Gneiss	Rowley et al. (1997)
244.0	4.7	SHRIMP	WMA	20	4.7	Granitic gneiss	Wan et al. (2005)
226.1	2.3	SHRIMP	WMA	17	0.7	Granitic gneiss	Wan et al. (2005)
219.4	1.4	SHRIMP	WMA-Mnz	23	1.2	Granitic gneiss	Wan et al. (2005)
217.8	1.7	SHRIMP	WMA-Mnz	–	–	–	Wan et al. (2005)
245.0	3.0	SHRIMP	WMA	8	0.2	Eclogite	Wu et al. (2006)
242.0	3.0	SHRIMP	WMA	8	0.4	Eclogite	Wu et al. (2006)
242.0	4.0	SHRIMP	WMA	4	0.6	Eclogite	Wu et al. (2006)
240.0	2.0	SHRIMP	WMA	13	0.8	Eclogite	Wu et al. (2006)
226.0	4.0	SHRIMP	WMA	4	0.5	Eclogite	Wu et al. (2006)
223.0	2.0	SHRIMP	WMA	11	1.4	Eclogite	Wu et al. (2006)
228.0	12.0	Conv	LIA	4	–	Orthogneiss	Zheng et al. (2003)
226.0	8.0	Conv	LIA	6	–	Orthogneiss	Zheng et al. (2003)
222.0	6.0	IMP-ICPMS	LIA	5	0.4	Orthogneiss	Zheng et al. (2004)
201.0	14.0	IMP-ICPMS	LIA	5	2.9	Orthogneiss	Zheng et al. (2004)
218.0	23.0	LA-ICPMS	LIA	–	–	Gneiss	Zheng et al. (2006)
216.0	30.0	LA-ICPMS	LIA	–	–	Eclogite	Zheng et al. (2006)
214.0	7.0	LA-ICPMS	LIA	–	–	Gneiss	Zheng et al. (2006)
214.0	36.0	ID-TIMS	LIA	–	–	Gneiss	Zheng et al. (2006)
213.0	22.0	LA-ICPMS	LIA	–	–	Gneiss	Zheng et al. (2006)
243.0	4.0	SHRIMP	LIA	10	0.0	Eclogite	Zheng et al. (2007)
224.0	3.0	SHRIMP	LIA	6	0.7	Eclogite	Zheng et al. (2007)
212.0	7.0	SHRIMP	LIA	11	2.1	Vein	Zheng et al. (2007)
210.0	4.0	LA-ICPMS	LIA	7	1.9	Vein	Zheng et al. (2007)

Note: Refer to note from Table A1.

References

Ames, L., Tilton, G.R., Zhou, G., 1993. Timing of collision of the Sino–Korean and Yangtse cratons: U–Pb zircon dating of coesite-bearing eclogites. Geology 21, 339–342.

Ames, L., Zhou, G., Xiong, B., 1996. Geochronology and isotopic character of ultrahigh-pressure metamorphism with implications for collision of the Sino–Korean and Yangtze cratons, central China. Tectonics 15, 472–489.

Ayers, J.C., Dunkle, S., Gao, S., Miller, C., 2002. Constraints on timing of peak and retrograde metamorphism in the Dabie Shan ultrahigh-pressure metamorphic

belt, east-central China, using U–Th–Pb dating of zircon and monazite. Chemical Geology 186, 315–331.
Chatelain, J.L., Roecker, S.W., Hatzfeld, D., Molnar, P., 1980. Microearthquake seismicity and fault plane solutions in the Hindu Kush region and their tectonic implications. Journal of Geophysical Research 85, 1365–1387.
Chavagnac, V., Jahn, B.-M., 1996. Coesite-bearing eclogites from the Bixiling Complex, Dabie Mountains, China: Sm–Nd ages, geochemical characteristics and tectonic implications. Chemical Geology 133, 29–51.
Chen, W.P., Nabelek, N., 1987. Seismogenic strike-slip faulting and the development of the North China basin. Tectonics 7, 975–989.
Chen, W., Li, Q., Li, D., Wang, X., 1989. Geochronological implications of K/Ar isotope system of fault gouge – preliminary study. Physics and Chemistry of the Earth 17, 17–23.
Chen, F., Siebel, W., Guo, J., Cong, B., Satir, M., 2003. Late Proterozoic magmatism and metamorphism recorded in gneisses from the Dabie high-pressure metamorphic zone, eastern China: evidence from zircon U–Pb geochronology. Precambrian Research 120, 131–148.
Chen, Y.-X., Zheng, Y.-F., Chen, R.-X., Zhang, S.-B., Li, Q., Dai, M., Chen, L., 2011. Metamorphic growth and recrystallization of zircons in extremely $_{18}$O-depleted rocks during eclogite-facies metamorphism: Evidence from U–Pb ages, trace elements, and O–Hf isotopes. Geochimica et Cosmochimica Acta 75, 4877–4898.
Cheng, H., King, R.L., Nakamura, E., Vervoort, J.D., Zhou, Z., 2008. Coupled Lu–Hf and Sm–Nd geochronology constrains garnet growth in ultra-high-pressure eclogites from the Dabie orogeny. Journal of Metamorphic Geology 26, 741–758.
Cheng, H., DuFrane, S.A., Vervoort, J.D., Nakamura, E., Zheng, Y.-F., Zhou, Z., 2010. Protracted oceanic subduction prior to continental subduction: new Lu–Hf and Sm–Nd geochronology of oceanic-type high-pressure eclogites in the western Dabie orogeny. American Mineralogist 95, 1214–1223.
Cheng, H., Vervoort, J.D., Li, X., Zhang, C., Li, Q., Zheng, S., 2011. The growth interval of garnet in the UHP eclogites from the Dabie orogenm China. American Mineralogist 96, 1300–1307.
Chung, S.-L., 1999. Trace element and isotope characteristics of Cenozoid basalts around the Tanlu fault with implications for the eastern plate boundary between north and south China. The Journal of Geology 107, 301–312.
Dunlap, W.J., 2003. Crystallization versus cooling ages of white micas: dramatic effect of K-poor inclusions on ^{40}Ar/^{39}Ar age spectra. Journal of the Virtual Explorer, 13.
Eide, E.A., McWilliams, M.O., Liou, J.G., 1994. ^{40}Ar/^{39}Ar geochronology and exhumation of high-pressure to ultrahigh-pressure metamorphic rocks in east-central China. Geology 22, 601–604.
Faure, M., Lin, W., Monié, P., Le Breton, N., Poussineau, S., Panis, D., Deloule, E., 2003. Exhumation tectonics of the ultrahigh-pressure metamorphic rocks in the Qinling orogen in east China: new petrological–structural–radiometric insights from the Shandong Peninsula. Tectonics 22, 1018. http://dx.doi.org/10.1029/2002TC001450.
Gao, C., Liu, Y., Zong, K., Hu, Z., Gao, S., 2010. Microgeochemistry of rutile and zircon in eclogites from the CCSD main hole: Implications for the fluid activity and thermo-history of the UHP metamorphism. Lithos 115, 51–64.
Gao, X.-Y., Zheng, Y.-F., Chen, Y.-X., 2011. U–Pb ages and trace elements in metamorphic zircon and titanite from UHP eclogite in the Dabie orogeny: constraints on P–T–t path. Journal of Metamorphic Geology 29, 721–740.
Gilder, S., Courtillot, V., 1997. Timing of the North-South China collision from new middle to late Mesozoic paleomagnetic data from the North China Block. Journal of Geophysical Research 102, 17,713–17,727.
Gilder, S.A., Zhao, X., Coe, R.S., Wu, H., Kuang, G., 1993. Discordance of Jurassic paleomagnetic data from south China and their tectonic implications. Earth and Planetary Science Letters 119, 259–269.
Gilder, S.A., Coe, R.S., Wu, H., Kunag, G., Zhao, X., Wu, Q., 1995. Triassic paleomagnetic data from south China and their bearing on the tectonic evolution of the western circum-Pacific region. Earth and Planetary Science Letters 131, 269–287.
Gilder, S.A., Leloup, P.H., Courtillot, V., Chen, Y., Coe, R.S., Zhao, X., Xiao, W., Halim, N., Cogné, J.-P., Zhu, R., 1999. Tectonic evolution of the Tancheng–Lujiang (Tan–Lu) fault via Middle Triassic to Early Cenozoic paleomagnetic data. Journal of Geophysical Research 104, 15,365–15,390.
Gong, B., Zheng, Y.-F., Wu, Y.-B., Zhao, Z.-F., Gao, T., Tang, J., Chen, R.-X., Fu, B., Liu, X., 2007. Geochronology and stable isotope geochemistry of UHP metamorphic rocks at Taohang in the Sulu orogen, east-central China. International Geology Review 49, 259–286.
Grimmer, J.C., Jonckheere, R., Enkelmann, E., Ratschbacher, L., Hacker, B.R., Blythe, A.E., Wagner, G.A., Wu, Q., Liu, S., Dong, S., 2002. Late Cretaceous–Cenozoic history of the southern Tan–Lu fault zone: apatite fission-track and structural constraints from the Dabie Shan (eastern China). Tectonophysics 359, 225–253.
Hacker, B.R., Wang, Q., 1995. Ar/Ar geochronology of ultrahigh-pressure metamorphism in central China. Tectonics 14, 994–1006.
Hacker, B.R., Ratschbacher, L., Webb, L., Shuwen, D., 1995. What brought them up? Exhumation of the Dabie Shan ultrahigh-pressure rocks. Geology 23, 743–746.
Hacker, B.R., Wang, X., Eide, E.A., Ratschbacher, L., 1996. The Qinling–Dabie ultra-high-pressure collisional orogeny. In: Yin, A., Harrison, T.M. (Eds.), The Tectonics of Asia. Cambridge University Press, pp. 345–370.
Hacker, B.R., Ratschbacher, L., Webb, L.E., Ireland, T., Walker, D., Dong, S., 1998. U/Pb zircon ages constrain the architecture of the ultrahigh-pressure Qinling–Dabie orogeny, China. Earth and Planetary Science Letters 161, 215–230.
Hacker, B.R., Ratschbacher, L., Webb, L.E., McWilliams, M.O., Ireland, T., Calvert, A., Dong, S., Wenk, H.-R., 2000. Exhumation of ultrahigh-pressure continental crust in east central China: Late Triassic–Early Jurassic tectonic unroofing. Journal of Geophysical Research 105, 13,339–13,364.
Hacker, B.R., Ratschbacher, L., Liou, J.G., 2004. Subduction, collision and exhumation in the ultrahigh-pressure Qinling–Dabie orogen. In: Malpas, J., Fletcher, C.J.N., Ali, J.R., Aitchison, J.C. (Eds.), Aspects of the Tectonic Evolution of China, vol. 226. Geological Society of London Special Publications, pp. 157–175.
Hacker, B.R., Wallis, S.R., Ratschbacher, L., Grove, M., Gehrels, G., 2006. High-temperature geochronology constraints on the tectonic history and architecture of the ultrahigh-pressure Dabie–Sulu orogeny. Tectonics 25, TC5006. http://dx.doi.org/10.1029/2005TC001937.
Hacker, B.R., Wallis, S.R., McWilliams, M.O., Gans, P.B., 2009. ^{40}Ar/^{39}Ar constraints on the tectonic history and architecture of the ultrahigh-pressure Sulu orogeny. Journal of Metamorphic Geology. http://dx.doi.org/10.1111/j.1525-1314.2009.00840.x.
Hsiao, L.-Y., Graham, S.A., Tilander, N., 2004. Seismic reflection imaging of a major strike-slip fault zone in a rift system: paleogene structure and evolution of the Tan–Lu fault system, Liaodong Bay, Bohai, offshore China. American Association of Petroleum Geologists Bulletin 88, 71–97.
Kimura, G., Takahashi, M., Kono, M., 1990. Mesozoic collision–extrusion tectonics in eastern Asia. Tectonophysics 181, 15–23.
Leech, M.L., Webb, L.E., Yang, T., 2006. Diachronous histories for the Dabie–Sulu orogen from high-temperature geochronology. In: Hacker, B.R., McClelland, W.C., Liou, J.G. (Eds.), Ultrahigh-pressure Metamorphism: Deep Continental Subduction, vol. 403. Geological Society of America Special Paper, pp. 1–22.
Li, Z.-X., 1994. Collision between the North and South China blocks: a crustal-detachment model for suturing in the region east of the Tanlu fault. Geology 22, 739–742.
Li, Z., Gerya, T.V., 2009. Polyphase formation and exhumation of high- to ultrahigh-pressure rocks in continental subduction zone: Numerical modeling and application to the Sulu ultrahigh-pressure terrane in eastern China. Journal of Geophysical Research 114, B09406. http://dx.doi.org/10.1029/2008JB005935.
Li, S., Xiao, Y., Liou, D., Chen, Y., Ge, N., Zhang, Z., Sun, S., Cong, B., Zhang, R., Hart, S.R., Wang, S., 1993. Collision of the North China and Yangtze and formation of coesite-bearing eclogites: Timing and processes. Chemical Geology 109, 89–111.
Li, S., Wang, S., Chen, Y., Liu, D., Qiu, J., Zhou, H., Zhang, Z., 1994. Excess argon in phengite from eclogite: evidence from dating of eclogite minerals by Sm–Nd, Rb–Sr, and ^{40}Ar/^{39}Ar methods. Chemical Geology 112, 343–350.
Li, S., Jagoutz, E., Lo, C.-H., Chen, Y., Li, Q., Xiao, Y., 1999. Sm/Nd, Rb/Sr, and ^{40}Ar/^{39}Ar isotopic systematics of the ultrahigh-pressure metamorphic rocks in the Dabie–Sulu belt, central China: a retrospective view. International Geology Review 41, 1114–1124.
Li, X.-P., Zheng, Y.-F., Wu, Y.-B., Chen, F., Gong, B., Li, Y.-L., 2004. Low-T eclogite in the Dabie terrane of China: petrological and isotopic constraints on fluid activity and radiometric dating. Contributions to Mineralogy and Petrology 148, 443–470.
Lin, S., 1995. Collision between the North and South China blocks: a crustal-detachment model for suturing in the region east of the Tanlu fault: comment and reply. Geology 23, 574–575.
Lin, J.-L., Fuller, M., 1990. Paleomagnetism, North China and South China collision, and the Tan–Lu fault. Philosophical Transactions of the Royal Society of London A 331, 589–598.
Lin, J.-L., Fuller, M., Zhang, W.-Y., 1985. Preliminary Phanerozoic polar wander paths for the North and South China blocks. Nature 313, 444–449.
Lin, W., Faure, M., Wang, Q., Monié, P., Panis, D., 2005. Triassic polyphase deformation in the Feidong–Zhangbaling Massif (eastern China) and its place in the collision between the North China and South China blocks. Journal of Asian Earth Sciences 25, 121–136.
Liou, J.G., Zhang, R.Y., Eide, E.A., Maruyama, S., Wang, X., Ernst, W.G., 1996. Metamorphism and tectonics of high-P and ultrahigh-P belts in Dabie–Sulu regions, eastern central China. In: Yin, A., Harrison, T.M. (Eds.), The Tectonic Evolution of Asia. Cambridge University Press, New York, pp. 300–343.
Liu, D., Jian, P., 2004. 243 Ma UHP and 228 Ma retrograde events of the Shuanghe jadeite quartzite, Eastern Dabie Mountains – SHRIMP dating, mineral inclusions and zircon REE patterns. Acta Geologica Sinica 78, 211–217 (in Chinese with English abstract).
Liu, F.L., Liou, J.G., 2011. Zircon as the best mineral for P–t-time history of UHP metamorphism: a review on mineral inclusions and U–Pb SHRIMP ages of zircons from the Dabie–Sulu UHP rocks. Journal of Asian Earth Sciences 40, 1–39.
Liu, F., Xu, Z., 2004. Fluid inclusions hidden in coesite-bearing zircons in ultrahigh-pressure metamorphic rocks from southwestern Sulu terrane in eastern China. Chinese Science Bulletin 49, 396–404.
Liu, F., Xu, Z., Liou, J.G., Song, B., 2004a. SHRIMP U–Pb ages of ultrahigh-pressure and retrograde metamorphism of gneisses, south-western Sulu terrane, eastern China. Journal of Metamorphic Geology 22, 315–326.
Liu, F., Xu, Z., Xue, H., 2004b. Tracing the protolith, UHP metamorphism, and exhumation ages of orthogneiss from the SW Sulu terrane (eastern China): SHRIMP U–Pb dating of mineral inclusion-bearing zircons. Lithos 78, 411–429.
Liu, X., Jahn, B.-M., Liu, D., Dong, S., Li, S., 2004c. SHRIMP U–Pb zircon dating of metagabbro and eclogites from western Dabieshan (Hong'an block), China, and its tectonic implications. Tectonophysics 394, 171–192.

Liu, F., Liou, J.G., Xu, Z., 2005. U–Pb SHRIMP ages recorded in the coesite-bearing zircon domains of paragneisses in the southwestern Sulu terrane, eastern China: new interpretations. American Mineralogist 90, 790–800.

Liu, D., Jian, P., Kroner, A., Xu, S., 2006a. Dating of prograde metamorphic events deciphered from episodic zircon growth in rocks of the Dabie–Sulu UHP complex, China. Earth and Planetary Science Letters 250, 650–666.

Liu, F.L., Gerdes, A., Liou, J.G., Xue, H.M., Liang, F.H., 2006b. SHRIMP U–Pb zircon dating from Sulu-Dabie dolomitic marble, eastern China: constraints on prograde, ultrahigh-pressure and retrograde metamorphic ages. Journal of Metamorphic Geology 24, 569–589.

Liu, F., Liou, J.G., Xue, H., 2006c. Identification of UHP and non-UHP orthogneisses in the Sulu UHP terrane, eastern China: evidence from SHRIMP U–Pb dating of mineral inclusion-bearing zircons. International Geology Review 48, 1067–1086.

Liu, F.L., Gerdes, A., Robinson, P.T., Xue, H., Ye, J., 2007. Zoned zircon from eclogite lenses in marbles from the Dabie–Sulu UHP terrane, China: a clear record of ultra-deep subduction and fast exhumation. Acta Geologica Sinica 81, 204–225.

Liu, F., Gerdes, A., Zeng, L., Xue, H., 2008. SHRIMP U–Pb dating, trace elements and the Lu–Hf isotope system of coesite-bearing zircon from amphibolite in the SW Sulu UHP terrane, eastern China. Geochimica et Cosmochimica Acta 72, 2973–3000.

Liu, F.L., Gerdes, A., Liou, J.G., Liu, P., 2009a. Unique coesite-bearing zircon from allanite-bearing gneisses: U–Pb, REE and Lu–Hf properties and implications for the evolution of the Sulu UHP terrane, China. European Journal of Mineralogy 21, 1225–1250.

Liu, F.L., Gerdes, A., Xue, H.M., 2009b. Differential subduction and exhumation of crustal slices in the Sulu HP–UHP metamorphic terrane: insights from mineral inclusions, trace elements, U–Pb and Lu–Hf isotope analyses of zircon in orthogneiss. Journal of Metamorphic Geology. http://dx.doi.org/10.1111/j.1525-1314.2009.00833.x.

Liu, S.S., Weber, U., Glasmacher, U.A., Xu, Z.Q., Wagner, G.A., 2009c. Fission track analysis and thermotectonic history of the main borehole of the Chinese Continental Scientific Drilling project. Tectonophysics 475, 318–326.

Liu, Y.-C., Gu, X.-F., Li, S.-G., Hou, Z.-H., Song, B., 2011. Multistage metamorphic events in granulitized eclogites from the North Dabie complex zone, central China: evidence from zircon U–Pb age, trace element and mineral inclusion. Lithos 122, 107–121.

Ma, C., Zhichang, L., Ehlers, C., Yang, K., Wang, R., 1998. A post-collisional magmatic plumbing system: mesozoic granitoid plutons from the Dabieshan high-pressure and ultrahigh-pressure metamorphic zone, east-central China. Lithos 45, 431–456.

Maruyama, S., Isozaki, Y., Kimura, G., Terabayashi, M., 1997. Paleogeographic maps of the Japanese Islands: plate tectonic synthesis from 750 Ma to the present. Island Arc 6, 121–142.

Maruyama, S., Tabata, H., Nutman, A.P., Morikawa, T., Liou, J.G., 1998. SHRIMP U–Pb geochronology of ultrahigh-pressure metamorphic rocks of the Dabie Mountains, central China. Continental Dynamics 3, 72–85.

Mattauer, M., Matte, P., Maluski, H., Xu, Z., Zhang, Q.W., Wang, Y.M., 1991. Paleozoic and Triassic plate boundary between North and South China; new structural and radiometric data on the Dabie-Shan (eastern China). Academie des Sciences Comptes Rendus, ser. II 312, 1227–1233.

Mercier, J.L., Hou, M., Vergély, P., Wang, Y., 2007. Structural and stratigraphical constraints on the kinematics history of the southern Tan–Lu fault zone during the Mesozoic Anhui Province, Chine. Tectonophysics 439, 33–66.

Okay, A.I., Sengor, A.M.C., 1992. Evidence for intracontinental thrust-related exhumation of the ultra-high-pressure rocks in China. Geology 20, 411–414.

Okay, A.I., Sengor, A.M.C., Satir, M., 1993. Tectonics of an ultrahigh-pressure metamorphic terrane: Dabie Shan, China. Tectonics 12, 1320–1334.

Qiu, H.-N., Wijbrans, J.R., Brouwer, F.M., Yun, J.-B., Zhao, L.-H., Xu, Y.-G., 2010. Amphibolite facies retrograde metamorphism of the Zhujiachong eclogite, SE Dabieshan: $^{40}Ar/^{39}Ar$ age constraints from argon extraction using UV-laser microprobe, *in vacuo* crushing and stepwise heating. Journal of Metamorphic Geology 28, 477–487.

Ratschbacher, L., Hacker, B.R., Webb, L.E., McWilliams, M., Ireland, T., Dong, S., Calvert, A., Chateigner, D., Wenk, H.-R., 2000. Exhumation of the ultrahigh-pressure continental crust in east central China: Cretaceous and Cenozoic unroofing and the Tan–Lu fault. Journal of Geophysical Research 105, 13303–13338.

Ratschbacher, L., Hacker, B.R., Calvert, A., Webb, L.E., Grimmer, J.C., McWilliams, M.O., Ireland, R., Dong, S., Hu, J., 2003. Tectonics of the Qinling (Central China): tectonostratigraphy, geochronology, and deformation history. Tectonophysics 366, 1–53.

Ratschbacher, L., Franz, L., Enkelmann, E., Jonckheere, R., Pörschke, A., Hacker, B.R., Dong, S., Zhang, Y., 2006. The Sino–Korean–Yangtze suture, the Huwan detachment, and the Paleozoic-Tertiary exhumation of (ultra)high-pressure rocks along the Tongbai–Xinxian–Dabie. In: Hacker, B.R., McClelland, W.C., Liou, J.G. (Eds.), Ultrahigh-pressure Metamorphism: Deep Continental Subduction, vol. 403. Geological Society of America Special Paper, pp. 45–75.

Reiners, P.W., Zhou, Z., Ehlers, T., Xu, C., Brandon, M.T., Donelick, R.A., Nicolescu, S., 2003. Post-orogenic evolution of the Dabie Shan, eastern China, from (U–Th)/He and fission-track thermochronology. American Journal of Science 303, 489–518.

Ren, J., Tamaki, K., Li, S., Zhang, J., 2002. Late Mesozoic and Cenozoic rifting and its dynamic setting in eastern China and adjacent areas. Tectonophysics 344, 175–205.

Riemann, A., Oberhänsli, R., Möller, A., Gerdes, A., Xu, Z., 2010. In situ LA-SF-ICP-MS U–Pb dating of metasomatic zircon growth during retrogression of UHP eclogites, Sulu deep drilling hole, China. European Journal of Mineralogy 21, 1251–1264.

Roecker, S.W., 1982. Velocity structure of the Pamir–Hindu Kush region: possible evidence of subducted crust. Journal of Geophysical Research 87, 945–959.

Rowley, D.B., Xue, F., Tucker, R.D., Peng, X., Baker, J., Davis, A., 1997. Ages of ultrahigh pressure metamorphism and protolith orthogneisses from eastern Dabie Shan: U/Pb zircon geochronology. Earth and Planetary Science Letters 151, 191–203.

Rumble, D., Giorgis, D., Ireland, T., Zhang, Z., Xu, H., Yui, T.F., Yang, J., Xu, Z., Liou, J.G., 2002. Low $\delta^{18}O$ zircons, U–Pb dating, and the age of the Qinglongshan oxygen and hydrogen isotope anomaly near Donghai in Jiangsu Province, China. Geochimica et Cosmochimica Acta 66, 2299–2306.

Schmidt, A., Weyer, S., Mezger, K., Scherer, E.E., Xiao, Y., Hoefs, J., Brey, G.P., 2008. Rapid eclogitisation of the Dabie–Sulu UHP terrane: constraints from Lu–Hf garnet geochronology. Earth and Planetary Science Letters 273, 203–213.

Schmidt, A., Mezger, K., O'Brien, P.J., 2011. The time of eclogite formation in the ultrahigh pressure rocks of the Sulu terrane: constraints from Lu–Hf garnet geochronology. Lithos 125, 743–756.

Sun, J., Chen, F., Wang, G., Jin, Y., 1993. Correlation between the Subei–Jiaonan and Dabie blocks and horizontal displacement of the Tancheng–Lujiang fault zone. In: Xu, J. (Ed.), The Tancheng–Lujiang Wrench Fault System. John Wiley and Sons, Ltd., pp. 97–104.

Tang, J., Zheng, Y.-F., Wu, Y.-B., Gong, B., Zha, X., Liu, X., 2008. Zircon U–Pb age and geochemical constraints on the tectonic affinity of the Jiaodong terrane in the Sulu orogen, China. Precambrian Research 161, 389–418.

Wallis, S., Enami, M., Banno, S., 1999. The Sulu UHP terrane: a review of the petrology and structural geology. International Geology Review 41, 906–920.

Wallis, S., Tsuboi, M., Suzuki, K., Fanning, M., Jiang, L., Tanaka, T., 2005. Role of partial melting in the evolution of the Sulu (eastern China) ultrahigh-pressure terrane. Geology 33, 129–132. http://dx.doi.org/10.1130/G20991.1.

Wan, Y., Li, R., Wilde, S.A., Liu, D., Chen, Z., Yan, L., Song, T., Yin, X., 2005. UHP metamorphism and exhumation of the Dabie orogen, China: evidence from SHRIMP dating of zircon and monazite from a UHP granitic gneiss cobble from the Hefei Basin. Geochimica et Cosmochimica Acta 69, 4333–4348.

Wang, X., Liou, J.G., Mao, H.K., 1989. Coesite-bearing eclogite from the Dabie Mountains in central China. Geology 17, 1085–1088.

Wang, W., Zhang, Z., Yu, F., Liu, F., Dong, X., Liou, J.G., 2011. Petrological and geochronologicalm constraints on the origin of HP and UHP kyanite-quartzites from the Sulu orogen, eastern China. Journal of Asian Earth Sciences 42, 618–632.

Wawrzenitz, N., Romer, R.L., Oberhänsli, R., Dong, S., 2006. Dating of subduction and differential exhumation of UHP rocks from the Central Dabie Complex (E-China): constraints from microfabrics, Rb–Sr and U–Pb isotope systems. Lithos 89, 174–201.

Webb, L.E., Hacker, B.R., Ratschbacher, L., McWilliams, M.O., Dong, S., 1999. Thermochronologic constraints on deformation and cooling history of high- and ultrahigh-pressure rocks in the Qinling–Dabie orogen, eastern China. Tectonics 18, 621–638.

Webb, L.E., Ratschbacher, L., Hacker, B.R., Dong, S., 2001. Kinematics of exhumation of high- and ultrahigh-pressure rocks in the Hong'an and Tongbai Shan of the Qinling–Dabie collisional orogen, eastern China. In: Hendrix, M.S., Davis, G.A. (Eds.), Paleozoic and Mesozoic Tectonic Evolution of Central Asia: From Continental Assembly to Intracontinental Deformation, vol. 194. Geological Society of America Memoir, pp. 231–245.

Webb, L.E., Leech, M.L., Yang, T., 2006. $^{40}Ar/^{39}Ar$ thermochronology of the Sulu terrane: Late Triassic exhumation of high and ultrahigh-pressure rocks and other implications for Mesozoic tectonics in East Asia. In: Hacker, B.R., McClelland, W.C., Liou, J.G. (Eds.), Ultrahigh-pressure Metamorphism: Deep Continental Subduction, vol. 403. Geological Society of America Special Paper, pp. 77–92.

Webb, L.E., Baldwin, S.L., Fitzgerald, P.G., Little, T.A., 2008. Can microplate rotation drive subduction inversion? Geology 36, 823–826.

Whitney, D.L., Evans, B.W., 2010. Abbreviations for names of rock-forming minerals. American Mineralogist 95, 185–187.

Wu, Y.-B., Zheng, Y.-F., Zhao, Z.-F., Gong, B., Liu, X., Wu, F.-Y., 2006. U–Pb, Hf and O isotope evidence for two episodes of fluid-assisten zircon growth in marble-hosted eclogites from the Dabie orogeny. Geochimica et Cosmochimica Acta 70, 3743–3761.

Xie, Z., Zheng, Y.-F., Jahn, B.-M., Ballevre, M., Chen, J., Gautier, P., Gao, T., Gong, B., Zhou, J., 2004. Sm–Nd and Rb–Sr dating of pyroxene–garnetite from North Dabie in east-central China: problem of isotope disequilibrium due to retrograde metamorphism. Chemical Geology 206, 137–158.

Xu, J.W., 1993. Basic characteristics and tectonic evolution of the Tancheng–Lujiang fault zone. In: Xu, J. (Ed.), The Tancheng–Lujiang Wrench Fault System. John Wiley and Sons, Ltd., pp. 17–50.

Xu, J., Zhu, G., 1994. Tectonic models of the Tan–Lu fault zone, eastern China. International Geology Review 36, 771–784.

Xu, Z., Zeng, L., Zhang, Z., Liu, F., Yang, J., Chen, F., Liang, F., McWilliams, M., Liou, J.G., 2006. Polyphase structural deformation and a dynamic model for the formation of Sulu high to ultrahigh-pressure (HP–UHP) metamorphic belt: from subduction to exhumation. In: Hacker, B.R., McClelland, W.C., Liou, J.G. (Eds.), Ultrahigh-pressure Metamorphism: Deep Continental Subduction, vol. 403. Geological Society of America Special Paper, pp. 93–113.

Xu, H., Ma, C., Ye, K., 2007. Early Cretaceous granitoids and their implications for the collapse of the Dabie orogen, eastern China: SHRIMP zircon U–Pb dating and geochemistry. Chemical Geology 240, 238–259.

Xu, Z., Yang, W., Ji, S., Zhang, Z., Yang, J., Wang, Q., Tang, Z., 2009. Deep root of a continent-continent collision belt: Evidence from the Chinese Continental Scientific Drilling (CCSD) deep borehole in the Sulu ultrahigh-pressure (HP–UHP) metamorphic terrane, China. Tectonophysics 475, 204–219.

Yang, J.S., Wooden, J.L., Wu, C.L., Liu, F.L., Xu, Z.Q., Shi, R.D., Katayama, I., Liou, J.G., Maruyama, S., 2003. SHRIMP U–Pb dating of coesite-bearing zircon from the ultra-high-pressure metamorphic rocks, Sulu terrane, east China. Journal of Metamorphic Geology 21, 551–560.

Yang, J.-H., Chung, S.-L., Wilde, S.A., Wu, F.-Y., Chu, M.-F., Lo, C.-H., Fan, H.R., 2005. Petrogenesis of post-orogenic syenites in the Sulu orogenic belt, east China: geochronological, geochemical and Nd–Sr isotopic evidence. Chemical Geology 214, 99–125.

Yin, A., Nie, S., 1993. An indentation model for the north and south China collision and the development of the Tan–Lu and Honam fault systems, eastern Asia. Tectonics 12, 801–813.

Yin, A., Nie, S., 1996. A Phanerozoic palinspastic reconstruction of China and its neighboring regions. In: Yin, A., Harrison, T.M. (Eds.), The Tectonics of Asia. Cambridge University Press, pp. 442–485.

Yu, F., Zhang, Z., Wang, W., Lui, F., Dong, X., Liou, J.G., 2011. Zircon U–Pb constaints on the origin of UHP meta-supracrustal rocks in the southern Sulu orogeny, eastern China. Journal of Asian Earth Sciences 42, 740–751.

Yuan, X.-C., Klemperer, S.L., Teng, W.-B., Liu, L.-X., Chetwin, E., 2003. Crustal structure and exhumation of the Dabie Shan ultrahigh-pressure orogen, eastern China, from seismic reflection profiling. Geology 31, 435–438.

Zhang, K.-J., 1997. North and South China collision along the eastern and southern North China margins. Tectonophysics 270, 145–156.

Zhang, R., Dong, S., Shi, W., 2003. Cretaceous deformation history of the middle Tan–Lu fault zone in Shandong Province, eastern China. Tectonophysics 363, 243–258.

Zhao, X., Coe, R.S., 1987. Palaeomagnetic constraints on the collision and rotation of North and South China. Nature 327, 141–144.

Zhao, X., Coe, R.S., 1989. Tectonic implications of Permo-Triassic paleomagnetic results from North and South China. Geophysical Monograph 50, 267–283.

Zhao, Z.-F., Zheng, Y.-F., Wei, C.-S., Wu, Y.-B., 2004. Zircon isotope evidence fro recycling of subducted continental crust in post-collisional granitoids from the Dabie terrane in China. Geophysical Research Letters 31, L22602. http://dx.doi.org/10.1029/2004GL021061.

Zhao, R., Liou, J.G., Zhang, R.Y., Wooden, J.L., 2005. SHRIMP U–Pb dating of zircon from the Xugou UHP eclogite, Sulu terrane, eastern China. International Geology Review 47, 805–814.

Zhao, R., Liou, J.G., Zhang, R.Y., Li, T., 2006a. SHRIMP U–Pb dating of the Rongcheng eclogite and associated peridotite: new constraints for ultrahigh-pressure metamorphism of mantle-derived mafic-ultramafic bodies from the Sulu terrane. In: Hacker, B.R., McClelland, W.C., Liou, J.G. (Eds.), Ultrahigh-pressure Metamorphism: Deep Continental Subduction, vol. 403. Geological Society of America Special Paper, pp. 115–125.

Zhao, Z.-F., Zheng, Y.-F., Gao, T.-S., Wu, Y.-B., Chen, B., Chen, F.-K., Wu, F.-Y., 2006b. Isotopic constraints on age and duration of fluid-assisted high-pressure eclogites-facies recrystallization during exhumation of deeply subducted continental crust in the Sulu orogeny. Journal of Metamorphic Geology 24, 687–702.

Zhao, R., Liou, J.G., Tsujimori, T., Zhang, R.Y., 2007a. Petrology and U–Pb SHRIMP geochronology of a garnet peridotite, Sulu UHP terrane, east-central China. International Geology Review 49, 732–752.

Zhao, R., Zhang, R.Y., Liou, J.G., Booth, A.L., Pope, E.C., Chamberlain, C.P., 2007b. Petrochemistry, oxygen isotopes and U–Pb SHRIMP geochronology of mafic–ultramafic bodies from the Sulu UHP terrane, China. Journal of Metamorphic Geology 25, 207–224.

Zheng, Y.-F., 2009. Fluid regime in continental subduction zones: petrological insights from ultrahigh-pressure metamorphic rocks. Journal of the Geological Society, London 166, 763–782.

Zheng, Y.-F., Wang, Z.-R., Li, S.-G., Zhao, Z.-F., 2002. Oxygen isotope equilibrium between eclogite minerals and its constraints on mineral Sm–Nd chronometer. Geochimica et Cosmochimica Acta 66, 625–634.

Zheng, Y.-F., Gong, B., Zhao, Z.-F., Fu, B., Li, Y.-L., 2003. Two types of gneisses associated with eclogite at Shuanghe in the Dabie terrane: carbon isotope, zircon U–Pb dating and oxygen isotope. Lithos 70, 321–343.

Zheng, Y.-F., Wu, Y.-B., Chen, F.-K., Gong, B., Li, L., Zhao, Z.-F., 2004. Zircon U–Pb and oxygen isotope evidence for a large-scale ^{18}O depletion event in igneous rocks during the Neoproterozoic. Geochimica et Cosmochimica Acta 68, 4145–4165.

Zheng, Y.-F., Zhao, Z.-F., Wu, Y.-B., Zhang, S.-B., Liu, X., Wu, F.-Y., 2006. Zircon U–Pb age, Hf and O isotope constratins on protolith origin of ultrahigh-pressure eclogite and gneiss in the Dabie orogeny. Chemical Geology 231, 135–158.

Zheng, Y.-F., Gao, T.-S., Wu, Y.-B., Gong, B., Liu, X.M., 2007. Fluid flow during exhumation of deeply subducted continental crust: zircon U–Pb age and O-isotope studies of a quartz vein within ultrahigh-pressure eclogite. Journal of Metamorphic Geology 25, 267–283.

Zhu, G., Wang, Y., Liu, G., Niu, M., Xie, C., Li, C., 2005. $^{40}Ar/^{39}Ar$ dating of strike-slip motion on the Tan–Lu fault zone, east China. Journal of Structural Geology 27, 1379–1398.

Zhu, G., Liu, G.S., Niu, M.L., Xie, C.L., Wang, Y.S., Xiang, B., 2007. Syn-collisional transform faulting of the Tan–Lu fault zone. East China International Journal of Earth Sciences. http://dx.doi.org/10.1007/s00531-007-0225-8, 21 p.

Zhu, G., Niu, M., Xie, C., Wang, Y., 2010. Sinistral to normal faulting along the Tan–Lu fault zone: evidence for geodynamic switching of the east China continental margin. The Journal of Geology 118, 277–293.

Zong, K., Liu, Y., Gao, C., Hu, Z., Gao, S., Gong, H., 2009. In situ U–Pb dating and trace element analysis of zircons in thin sections of eclogites: refining constraints on the ultra high-pressure metamorphism of the Sulu terrane, China. Chemical Geology. http://dx.doi.org/10.1016/j.chemgeo.2009.09.021.